Conservation of molecular responses upon viral infection in the non-vascular plant *Marchantia polymorpha*

Eric Ros-Moner [1*], Tamara Jiménez-Góngora[1*], Luis Villar-Martín[1], Lana Vogrinec[2,3], Víctor M. González-Miguel[4], Denis Kutnjak[2] and Ignacio Rubio-Somoza[1,5]

[1]Molecular Reprogramming and Evolution (MoRE) Laboratory, Centre for Research in Agricultural Genomics (CRAG), CSIC-IRTA-UAB-UB, Campus UAB-Edifci CRAG. 08193 Cerdanyola del Vallés, Spain.

[2]National Institute of Biology, Department of Biotechnology and Systems Biology, Ljubljana, Slovenia.

[3]Jožef Stefan International Postgraduate School, Ljubljana, Slovenia.

[4]Data Analysis area, Bioinformatics Core Unit, Centre for Research in Agricultural Genomics (CRAG), CSIC-IRTA-UAB-UB, Campus UAB-Edifci CRAG. 08193 Cerdanyola del Vallés, Spain.

[5]Consejo Superior de Investigaciones Científicas (CSIC), Barcelona 08001, Spain.

*Those authors contributed equally to this work

To whom correspondence should be addressed: Ignacio.rubio@cragenomica.es

Abstract

After plants transitioned from water to land around 450 million years ago, they faced novel pathogenic microbes. Their colonization of diverse habitats was driven by anatomical innovations like roots, stomata, and vascular tissue, which became central to plant-microbe interactions. However, the impact of these innovations on plant immunity and pathogen infection strategies remains poorly understood. Here, we explore plant-virus interactions in the bryophyte *Marchantia polymorpha* to gain insights into the evolution of these relationships. Virome analysis reveals that *Marchantia* is predominantly associated with RNA viruses. Comparative studies with tobacco mosaic virus (TMV) show that *Marchantia* shares core defense responses with vascular plants but also exhibits unique features, such as a sustained wound response preventing viral spread. Additionally, general defense responses in Marchantia are equivalent to those restricted to vascular tissues in Nicotiana, suggesting that evolutionary acquisition of developmental innovations results in re-routing of defense responses in vascular plants.

31 **Introduction**

32 It is estimated that plants developed a functional vascular system through repurposing of pre-
33 existing genes around 420 million years ago, which facilitated the growth of larger plants by
34 providing mechanical support and enabling long distant transport of water, nutrients, and
35 signalling molecules (Bowles et al., 2022, Lucas et al., 2013). Viruses are obligate parasites that
36 can infect virtually any living organism hijacking central host cellular functions to replicate and
37 spread within and intra hosts. Coincidentally with land colonization, the repertoire of viruses
38 (virome) associated to plants enlarged and diversified both in nature and infection strategies.
39 Although our current knowledge lacks information on virome composition at intermediately
40 divergent plant lineages, it appears that viruses with large DNA genomes majorly infecting
41 unicellular chlorophyte algae were displaced by an increasing population of viruses with RNA
42 and small DNA genomes found in vascular plants (Mushegian et al., 2016). Plant vasculature has
43 become central for the success of viral infections in tracheophytes, not only serving as fast track
44 for viral systemic spread, but also providing a unique cellular environment for some viruses
45 which replication is restricted to that tissue (Kappagantu et al., 2020). Accordingly, vascular cells
46 are thought to present specific responses to viral infection when compared to other leaf cell-
47 types (Collum and Culver, 2017).

48 Our current understanding of the molecular events governing plant-virus interactions is vastly
49 shaped by studies focusing on vascular plants, mainly crops. Plants respond to viral infections via
50 at least three different but interconnected defense mechanisms (Mandadi and Scholthof, 2013).
51 Firstly, plants have an extracellular surveillance system that monitors the presence of pathogens
52 through the recognition of highly conserved microbe patterns dubbed as Pattern-associated
53 molecular patterns (PAMPs), such as viral derived double-strand RNAs (dsRNAS), the bacterial
54 flagellin or the fungal chitin. Detection of those molecules by specialized surface-localized
55 receptor kinases (Pattern recognition receptors, PRRs), triggers a first layer of defense called
56 PAMP-triggered immunity (PTI). PRRs expression is often restricted to focal points for microbial
57 interaction and invasion (Beck et al., 2014, Yotsui et al., 2023). Two additional surveillance
58 mechanisms monitor the intracellular presence of microbe-derived molecules. Highly stable
59 dsRNAs produced by viruses during their life cycle, independently of the DNA or RNA nature of
60 their genomes, are detected by the RNA silencing machinery which constitutes a conserved
61 antiviral defense mechanism both in plants and animals (Ding et al., 2018, Ding and Voinnet,
62 2007). Additionally, RNA silencing machinery also recognizes dsRNA generated from the

63 conversion of exogenous and endogenous single strand RNAs (ssRNA) by RNA-dependent RNA
64 polymerases (RDRs). RDR1 and RDR6 have been involved in antiviral defense in *Arabidopsis*
65 *thaliana* and *Nicotiana tabacum* (Garcia-Ruiz et al., 2010, Rakhshandehroo et al., 2017, Ying et
66 al., 2010), even though *Nicotiana benthamiana* has only a functional RDR6 (Bally et al., 2015).
67 Upon recognition, viral dsRNAs are trimmed in small RNAs (visRNAs) of 21 to 24 nucleotides in
68 length by members of the DICER-like family, mainly DCL2, DCL3 and DCL4 in Arabidopsis and
69 Nicotiana (Garcia-Ruiz et al., 2010, Lewsey and Carr, 2009). The resulting visRNA duplexes are
70 subsequently loaded into proteins from the ARGONAUTE family, which are the core elements of
71 the RNA-induced silencing complex (RiSC), and used to scan the intracellular space for the source
72 of dsRNA precursors in a sequence complementary manner abrogating viral infection (Lopez-
73 Gomollon and Baulcombe, 2022). In turn, viruses produce countermeasures, known as silencing
74 suppressors, targeted to interfere with different steps of the host RNA silencing machinery
75 (Lopez-Gomollon and Baulcombe, 2022). In response to these silencing suppressors, host micro
76 RNAs (miRNA, one of the two main classes of endogenous sRNAs in plants) are no longer
77 functional, allowing the translation of their targets and licensing a new layer of defense. Among
78 the miRNA targets involved in such counter-counter measure, members of the Nucleotide-
79 binding domain leucine-rich repeat (NLR) family are central. Thus, it has been suggested that
80 host miRNAs might work as sensors for the presence of pathogen-derived silencing suppressors
81 enabling a rapid host defense response based on the activation of otherwise silenced miRNA
82 targets (Vasseur et al., 2022, Silvestri et al., 2024). NLRs are core elements of the third
83 intracellular surveillance system for directly monitoring the intracellular presence of pathogen-
84 derived molecules, such as the prototypical case of the tobacco mosaic virus (TMV) replicase by
85 the gene *N* in tobacco (Erickson et al., 1999), or their impact on host cellular homeostasis. NLR-
86 activation triggers the so-called Effector-triggered immunity (ETI), which normally leads to a
87 hypersensitive response (HR) culminating in cell death. Those three defense systems, PTI, RNA
88 silencing and ETI largely rely on the action of the plant hormone Salicylic acid (SA). PTI and ETI
89 responses encompass activation of SA signalling (Pruitt et al., 2021) while SA activates RDR1 in
90 Arabidopsis and Nicotiana (Lee et al., 2016, Ying et al., 2010, Yu et al., 2003). Additionally, RDR1
91 expression is also induced by treatment with jasmonates (Liu et al., 2009, Xu et al., 2013),
92 another central hormone in plant defense. Many of those immunity components and networks
93 were already present in the last common land plant ancestor, while others have been acquired
94 alongside the increasing plant cellular and anatomical complexity (de Vries et al., 2018, Belanger
95 et al., 2023, Chia et al., 2024b).

96 A central question in plant-microbe interactions is how the evolution of different plant
97 developmental trajectories, including the acquisition of major innovations, impacts host defense
98 and pathogen infection strategies. In animals, comparative studies have proved very informative
99 about the origin and diversification of their innate immune responses against virus (Iwama and
100 Moran, 2023). Likewise, comparative studies including non-vascular plants, like the liverwort
101 *Marchantia polymorpha*, have been instrumental in understanding the evolution of the
102 interactions between plants and pathogens other than viruses (Carella et al., 2018, Gimenez-
103 Ibanez et al., 2019, Redkar et al., 2022). Comparative studies in plants have traditionally relied
104 on both model plant species and microbes, despite the lack of prior experimental evidence for
105 those interactions to occur in nature. Incorporating bryophytes into those comparative studies
106 not only provides important information on how plant immune programs may have evolved, but
107 it also bears the potential to determine the contribution of developmental innovations, such as
108 roots, stomata or vasculature, to their diversification.

109 To enable comparative studies towards understanding the evolution of plant-virus interactions,
110 we here characterized the molecular interplay between the non-vascular liverwort *Marchantia*
111 *polymorpha* and viruses. We firstly defined the composition of the virome of Marchantia plants
112 living in the wild and used that information to select a virus with similar genomic features to
113 those found in nature for further molecular characterization, and which could be tagged with a
114 fluorescent protein that enables monitoring of infection. Additionally, the selected virus should
115 be able to infect a broad range of hosts, in which their molecular interactions have been studied.
116 Following those criteria, we focused on the first ever isolated virus, the tobacco mosaic virus
117 (TMV). TMV is a ssRNA virus from the Tobamovirus genus showing a broad host range in nature
118 (Zamfir et al., 2023). Additionally, TMV has been extensively used for studying plant-virus
119 interactions in a wealth of plant species, including several Solanaceae species, like tomato and
120 tobacco, and the model plant *Arabidopsis thaliana*, which provide strong foundation for
121 comparative studies. TMV infects through wound entry points from where it moves cell-to-cell
122 via plasmodesmata, until it reaches the vascular system for systemic infection of distal parts of
123 the plant following the stream of photoassimilates (Liu and Nelson, 2013).

124 Our results show that *Marchantia polymorpha* is associated with RNA viruses in natural
125 populations that can replicate in lab grown Marchantia plants. Additionally, TMV can replicate in
126 Marchantia plants triggering a conserved transcriptional reprogramming encompassing
127 increased wounding and PTI responses in detriment of photosynthesis and cell cycle progression

128 and leading to changes in life-history traits, such as aging and senescence. Induction of a wealth
129 of NLR proteins and core elements from the RNA silencing machinery were also observed,
130 including DCL4 that, in absence of a DCL2 gene in the Marchantia genome (Belanger et al., 2023),
131 seems to be the main antiviral DCL protein according to the predominant 21 nuleotides in length
132 presented by TMV-derived vsRNAs. Noteworthy, the general response of the RNA silencing
133 machinery observed in Marchantia upon TMV infection is equivalent to that found specifically in
134 vascular tissues of *Nicotiana benthamiana*, suggesting an evolutionary anatomical rerouting of
135 antiviral defense towards newly acquired focal points for viral infection.

136 We additionally identified a conserved host interactor with the TMV silencing suppressor p126
137 that triggers cross-species defense against TMV.

138 **Results**

139 ***Marchantia polymorpha* is associated to RNA viruses in nature.**

140 To identify viruses associated with *Marchantia polymorpha* in nature, we performed a
141 virome analysis of two composite plant samples including 21 individuals growing naturally, not
142 cultivated, in 5 different locations spanning 4 different countries and accessible to possible viral
143 vectors. First included Marchantia individuals obtained from three open air botanical gardens
144 throughout Europe: Tübingen (Germany), Bern (Switzerland) and Cambridge (UK). The second
145 encompassed individuals growing open air at the botanical garden in Osnabrück (Germany) and
146 individuals growing in urban sites in Ljubljana (Slovenia). In addition to the expected background
147 of bacteriophage sequences, we detected several known viruses, including some capable of
148 infecting or being associated with plants, fungi or invertebrates (Supplementary Data 1).
149 Putatively new virus-like sequences, possibly associated with *M. polymorpha*, were selected for
150 further analyses from the first dataset, based on i) their relatively high average sequencing
151 depths and ii) similarity to viruses previously associated with eukaryotic organisms, including
152 plants and invertebrates (Supplementary Data 2). Two previously described and three newly
153 identified viruses were hence selected for further RT-qPCR confirmation of their association with
154 the different *M. polymorpha* individuals, along with plants from the Tak-1 reference accession
155 grown in sterile conditions. Specific primers to detect Ligustrum necrotic ringspot virus (LNRV,
156 known to infect plants), Hubei picorna-like virus 51, (detected in a metagenomics study and
157 putatively associated with diverse sample types by datamining – see results below) a newly
158 identified picorna-like virus (which we named Tübingen picorna-like virus 1, with average

159 mapping depth of 2230x and contig length of 7801 nts), a new tombus-like virus (Tübingen
160 tombus-like virus 1, with average mapping depth of 218x and contig length of 4521 nts), and a
161 new sobemo-like virus (Bern sobemo-like virus 1, with average mapping depth of 88x and contig
162 length of 2569 nts) were used for these analysis. While none of those viruses were detected in
163 negative control Tak-1 plants, individuals from Tübingen were associated with all tested viruses
164 but the Bern sobemo-like virus 1, which in turn was present in individuals from Bern along with
165 Tübingen picorna-like virus 1. Individuals from the Cambridge population were associated with
166 Hubei picorna-like virus 51 and Tübingen picorna-like virus 1 (Supplementary Data 3). Further,
167 we used a datamining approach to search for the presence of conserved RdRp domain
168 fingerprints (palmprints) of the selected viruses in global short reads sequence datasets using
169 Serratus infrastructure (Edgar et al., 2022). The results of the analysis suggested that palmprint
170 RdRp sequences with high similarity to those of queried viruses, can be associated with diverse
171 sample types, mostly including environmental samples, such as wastewater, water, rhizosphere,
172 soil and plants (Supplementary Data 4).

173 Given that Tübingen picorna-like virus 1 was present in all tested populations from the first
174 sampling, we decided to further characterize its genomic features and interaction with
175 *Marchantia polymorpha*. Indeed, Tübingen picorna-like virus 1 had the highest mapping depth
176 of all contigs in our virome analysis and showed a similar genome structure as other unclassified
177 picorna-like viruses (Shi et al., 2016), consisting of two predicted genome open reading frames
178 (ORFs), first containing domains with homology to superfamily 3 helicase, peptidase C3 and RNA-
179 dependent RNA polymerase (RdRp) and second three domains with homology to a coat protein
180 with 8-stranded jelly roll β-barrel motif (Figure 1A). Phylogenetic analysis (Figure 1B) of the RdRp
181 protein sequence and its closest NCBI GenBank homologues showed high similarity (80% identity
182 of aligned sequences) of this virus isolate with a recently reported plant associated picorna-like
183 virus (Trichosanthes kirilowii picorna-like virus, QKK82970.1). Much lower identities were
184 observed for Tübingen picorna-like virus 1 (29-42%) and other viruses associated with diverse
185 sources (plants, gastropods, water, crayfish, artropods and bird feces). However, given that they
186 were discovered in metagenomics studies their association with these hosts is only speculative.
187 Thus, we performed and additional phylogenetic analysis, comparing the RdRp sequence of
188 Tübingen picorna-like virus 1 with most similar RdRp sequences from RNA Viruses in
189 Metatranscriptomes (RVMT) database (https://riboviria.org/) (Neri et al., 2022). The analysis
190 revealed high similarity of the viral RdRp to several sequences included in family-level cluster

191 f.0032 with order *Picornavirales* (Supplementary Fig. 1A). Even if this cluster contains diverse
192 representatives, none of those has confirmed host associations to the date (Supplementary Data
193 5). Similarly, as found in Serratus analysis, sequences most similar to investigated virus were
194 associated, e.g., with wastewater, wetlands, and peat soil samples (Supplementary Fig. 1b,
195 Supplementary Data 5).

196 Next, we tested whether the Tübingen picorna-like virus 1 was able to replicate in *M. polymorpha*
197 by incubating two-weeks old Tak-1 individuals with extracts isolated from the Tübingen
198 population, which contained the highest levels of Tübingen picorna-like virus 1, as determined
199 by RT-qPCR analysis, or from Tak-1 plants grown in sterile conditions. Individual Marchantia
200 plants were collected one and two weeks after incubation and the levels of viral accumulation
201 were measured by RT-qPCR. Individuals exposed to extracts from virus-positive plants showed a
202 trend of increased viral levels over time, while no amplification was observed in plants incubated
203 with extracts from Tak-1 plants (Figure 1C). This indicated that Tübingen picorna-like virus 1 can
204 replicate in Marchantia.

205 Collectively, those results show that *Marchantia polymorpha* can be associated with RNA viruses
206 in nature.

207 Additionally, we performed data mining to search for possible DNA viruses associated with
208 *Marchantia polymorpha*. Sequencing data from 74 biological samples (obtained from natural
209 environments; (Beaulieu et al., 2023)) was analyzed for the presence of viral contigs. Analysis
210 revealed that most of the examined samples contained virus-like sequences, with the majority
211 exhibiting similarity to bacteriophages (Supplementary Data 6). Within the dataset we also found
212 virus-like sequences with similarity to members of *Phycodnaviridae,* which can infect unicellular
213 green algae. Since only few relatively short contig sequences for this group of viruses were
214 identified in different datasets, and the data was primarily not produced with microbiome study
215 in mind (e.g., no surface washing) the association with *M. polymorpha* with viruses from this
216 taxon is dubious and shall be further explored in future studies.

217 **Tobacco mosaic virus replicates in *Marchantia polymorpha***

218 Since its identification in the 19th century, tobacco mosaic virus has been extensively used for
219 studying plant-virus interactions in several vascular plant species like Arabidopsis and Nicotiana
220 (Scholthof, 2004). As a first step for comparative studies on plant-virus interactions between
221 vascular and non-vascular plants, we aimed to infect *Marchantia polymorpha* plants with a GFP

222 labelled clone of TMV (Peart et al., 2002). Sap from leaves of healthy and infected *Nicotiana*
223 *benthamiana* plants were isolated and used to incubate two-week-old Tak-1 plants grown in
224 sterile conditions. After incubation, Marchantia plants were transferred to soil and part of the
225 remaining sap was mechanically inoculated with an abrasive (carborundrum) in basal leaves
226 from 1 month old Nicotiana plants, as control for its infectivity. After two weeks, Nicotiana plants
227 showed systemic GFP signal under UV light along with symptoms of infection (Supplementary
228 Fig. 2), whereas Tak-1 plants displayed GFP signal in discrete infection foci that increased their
229 size over time (Figure 2A, Supplementary Fig. 3), suggestive of viral replication. This was further
230 corroborated by RT-qPCR amplification of pooled samples including four GFP positive individuals
231 at the first (T1) and second weeks after incubation (T2), in comparison with mock and freshly
232 incubated (T0) plants (Figure 2B, Supplementary Fig. 4). sRNA profiling in GFP positive areas from
233 Marchantia thalli identified TMV-derived vsRNAs enriched in 21 nucleotides long fragments,
234 consistent with DCL4-mediated processing, and mapping to the TMV-GFP sequence (Figure 2C,
235 Supplementary Fig. 5).

236 Histological sections of the infected area showed presence of the virus in all cell types, as inferred
237 from GFP fluorescence and when compared to sections from mock treated plants, suggesting no
238 preference for a specific cell-type during viral infection (Figure 2D).

239 Those results confirmed that TMV can replicate in *M. polymoprha* plants pointing to Marchantia-
240 TMV as a suitable pathosystem for comparative studies.

241 **TMV infection triggers profound molecular reprogramming in *M. polymoprha***

242 To characterize the molecular reprogramming caused by TMV infection, we performed
243 transcriptomic assays. TMV-GFP infected tissue from 4-week-old Marchantia plants (2 weeks
244 after inoculation) was collected in four pools including samples from 5 plants each, along with
245 the very same area from mock treated plants as control (Supplementary Fig. 6A). RNA was
246 isolated and the presence of TMV was confirmed by RT-qPCR in each pool (Supplementary Fig.
247 6B). Principal component analysis (PCA, Supplementary Fig. 6C) of the transcriptome supported
248 the RT-qPCR results showing a clear separation of infected and mock samples. Since separation
249 among infected samples correlated with viral RT-qPCR levels, we selected the three replicates
250 that had the highest levels of TMV and clustered together for further analysis. A total of 1879
251 genes were found to be up regulated while 1645 were reduced (padjust<0.05, Log2(fold-change)
252 =>1 or <-1) in response to TMV infection (Supplementary Data 7). Consistently with an ongoing

253 pathogenic interaction, we found several defense related marker genes among the differentially
254 expressed genes (DEG). Members of the pathogenesis-related (PR) family are prime markers of
255 immune responses in several plant species, including Marchantia (Carella et al., 2019, Gimenez-
256 Ibanez et al., 2019) and we found that the expression of several homologues showed opposite
257 expression profiles when compared to mock treated plants (Supplementary Table 1). Several PTI
258 marker genes have been identified in Marchantia based on their orthology to those established
259 in Arabidopsis (Gimenez-Ibanez et al., 2019) and their activation in the presence of bacterial and
260 fungal extracts (Gimenez-Ibanez et al., 2019, Redkar et al., 2022). We observed that a set of those
261 conserved PTI markers were also induced in response to TMV infection (Figure 3A). Additionally,
262 a significant number of intracellular receptors from the NLR family displayed upregulated
263 expression upon TMV infection ($p < 6.245e-05$ with those described by (Bowman et al., 2017); p
264 $< 1.308e-05$ with those described by (Chia et al., 2024); Supplementary Table 2). Nevertheless,
265 in line with the absence of TNL genes in Marchantia (Chia et al., 2024), none of those showed
266 significant sequence similarity to the NLR N gene triggering ETI responses in TMV infected
267 tobacco plants (Whitham et al., 1994). Likewise, several components from the RNA silencing
268 machinery upregulated in tobacco plants upon TMV infection (Sheng et al., 2019), were also
269 differentially expressed in response to TMV in Marchantia plants. The non-canonical MpDCL1b
270 (Mp6g09830), MpDCL4 (Mp7g11720), and MpRDR6 (Mp8g14970) were upregulated, whereas
271 MpDCL3 (Mp1g02840), MpAGO9 (Mp8g08610) and MpNRPE1b (Mp6g00230) were suppressed.

272 Gene Ontology (GO) analysis of the upregulated genes revealed an enrichment (padjust<0.05)
273 of biological processes related to reactive oxygen species, wounding, light intensity, heat
274 responses and responses to fungus and the presence of their constituent chitin (Supplementary
275 Data 8, Supplementary Fig. 7A). Photosynthesis, DNA packaging and cell cycle, microtubule
276 organization or regulation of salicylic acid metabolism were among the downregulated processes
277 (padjust<0.05; Supplementary Data 9, Supplementary Fig. 7B).

278 Notably, TMV is mainly transmitted through wounds and wounding response was one of the
279 processes to which upregulated genes belonged in the GO analysis, which prompted us analysing
280 this response. ERF transcription factors are central to trigger wounding responses in vascular
281 plants such as *A. thaliana* (Heyman et al., 2018) with a conserved set of ERF transcription factors
282 being also recently described to respond to wounding in *Marchantia polymorpha* plants (Liang
283 et al., 2022). A subset of these wounding responsive ERF transcription factors showed the same
284 expression pattern upon TMV infection as that observed upon intensive wounding (Figure 3B,

285 (Liang et al., 2022). To determine the whole transcriptional overlap between wounding and TMV
286 responses, we reanalysed published tissue incision transcriptomic responses (Liang et al., 2022)
287 using the same pipeline we used for the TMV samples. Comparison of both datasets showed a
288 significant overlap both in up-regulated (593 genes; $p<6.631e-235$) and down-regulated genes
289 (162 genes; $p<2.137e-70$; Figure 3C), suggesting that TMV infection might contribute to a
290 sustained wound response in Marchantia.

291 Chitin is one of the most abundant polysaccharides in nature and it is a primary component of
292 cell walls in fungi and exoskeletons of arthropods such as insects, which in turn can work as viral
293 vectors in a range of plants species (Campbell, 1996). According to the GO enrichment in
294 response to chitin and fungi, and besides the fungal responsive genes described above as part
295 of a conserved PTI response, we also observed upregulation of a set of fungal responsive WRKY
296 transcription factors (Figure 3D; (Redkar et al., 2022, Yotsui et al., 2023).

297 Photosynthetic deficiency is a hallmark for several stress responses, including those involving
298 viral infections. Accordingly, downregulation of transcripts involved in photosynthesis was one
299 of the main processes affected in our GO study as consequence of TMV infection. We determined
300 the photosynthetic efficiency in TMV infected areas from 4-weeks old Tak-1 plants after 2-weeks
301 of infection along with the very same area in mock treated plants. TMV infected areas showed a
302 significant reduction in photosynthetic competency when compared to similar areas from mock
303 treated plants (Figure 3E). Notably, parts of those very same plants distant to the infection foci,
304 showed also reduced photosynthetic capability, although to a lesser extent (Figure 3F). Those
305 results suggest that TMV responses might be systemic in *Marchantia polymorpha* plants.

306 Overall, those results show that TMV engages in a compatible interaction with *Marchantia*
307 *polymorpha*.

308 **Salicylic and OPDA-dependent signaling pathways are active at TMV infected areas.**

309 The plant hormones Salicylic acid (SA) and Jasmonic acid (JA) are central in defense responses
310 against most pathogens of vascular plants, acting both in a synergistic and antagonistic manner.
311 Whereas the SA biosynthesis and signalling pathway are mostly conserved in *Marchantia*
312 *polymoprha* (Jia et al., 2023), the active molecules binding to the COI1 receptor and triggering
313 jasmonate signaling are a group of long chain polyunsaturated fatty acids, including dinor-OPDA,
314 instead of JA-Ile (Kneeshaw et al., 2022, Monte et al., 2018). Therefore, we compared the SA and
315 jasmonate-related transcriptomic responses with those found during TMV infection. To that end,

316 we used the time course datasets obtained on incubation of Marchantia with 1mM SA during 2,
317 6 and 12 hours (Jeon et al., 2022), SA concentration shown to promote defense against bacterial
318 and to increase susceptibility to fungal pathogens (Jeon et al., 2022, Matsui et al., 2020).
319 Comparison of the DEGs identified on SA treatment showed a significant overlap with those
320 responding to TMV infection (Figure 4A; Supplementary Fig. 8). A total of 225 genes were
321 commonly up-regulated by 2 hours SA treatment or TMV ($p<1.799e-100$), 306 ($p < 1.382e-172$)
322 were shared after 6 hours treatment, and 92 ($p < 3.580e-47$) by 12 hours of SA incubation.
323 Likewise, TMV infection shared 47 down regulated genes ($p<1.618e-14$) with 2 hours, 38 ($p <$
324 $2.897e-13$) with the 6 hours, and 17 genes with 12 hours incubation samples ($p < 1.720e-05$),
325 showing that TMV infection activates SA-dependent transcriptional responses.

326 To ascertain a possible contribution of the jasmonate signalling pathway, we compared the TMV
327 transcriptional response with that of plants treated with dn-OPDA (Monte et al., 2018) or having
328 a constitutively active jasmonate pathway as a consequence of the mutation of the JAZ signalling
329 repressor (Mpjaz-1 KO plants; (Monte et al., 2019). A total of 143 and 81 genes were commonly
330 up-regulated upon TMV infection and *MpJAZ* deficiency or dn-OPDA treatment, while 238 were
331 downregulated in TMV infected and Mpjaz-1 KO plants (Figure 4B), suggesting that TMV infection
332 also activates the jasmonate signalling pathway in Marchantia. Finally, we found that 64 genes
333 were commonly up-regulated by TMV infection, SA 6 h treatment and absence of a functional
334 MpJAZ protein, while 54 genes were up-regulated by TMV infection, SA 6h and dn-OPDA
335 treatments (Figure 4C).

336 Next, we performed a GO analysis in the different sets of genes that were found to be commonly
337 regulated by TMV infections and each of the different hormone-related transcriptomes (i.e. Up
338 regulated genes by TMV and SA 6 h treatment from Figure 4A). That approach showed that the
339 JA pathway might contribute to the activation of wounding, reactive oxygen species and virus
340 responses, in addition to the catabolism of several compounds, including lipids,
341 phenylpropanoids and salicylic acid, in TMV infected Marchantia plants. Interestingly, some of
342 these processes were also commonly upregulated by TMV infection and SA treatment, including
343 wounding, SA and lignin catabolism among others. The SA response pathway might on the other
344 side also contribute to the observed transcriptional up-regulation of defense genes against
345 bacteria and fungi, as well as response to chitin in TMV infected plants (Figure 4D,
346 Supplementary Data 10). Amongst the downregulated processes by MpJAZ deficiency and TMV
347 infection were translational elongation, mucilage and cell wall biosynthesis, response to

348 fructose, photosynthesis, microtubule-based process, growth, and response to abscisic acid
349 (ABA; Figure 4E, Supplementary Data 10)

350 Furthermore, genes found to be commonly upregulated by TMV, SA and dn-OPDA treatment
351 were related to oxylipin and phenylalanine metabolism, wounding and drought recovery, among
352 other Gene ontology groups (Figure 4F; Supplementary Data 11). Meanwhile, those genes found
353 to be commonly upregulated by TMV infection, SA 6 h treatment and enhanced JA signalling in
354 Mpjaz-1 plants were related to antiviral defense and lipid catabolism, which has been also
355 recently found to contribute to SA activation and antiviral defense (Xu et al., 2022); Figure 4G,
356 Supplementary Data 11).

357 Collectively, those results suggest that SA and JA signalling pathways are activated in Marchantia
358 during TMV infection.

359 **TMV infection triggers aging in *Marchantia polymorpha.***

360 Interactions with pathogens, including viruses, can result in the modification of life-history traits
361 and developmental trajectories both in plants and animal (Pagan et al., 2008, Sievert, 1978).
362 Senescence is the final stage of the life cycle of a cell, tissue or organism and it is gradually
363 triggered throughout aging. This process can be accelerated by the interaction with different
364 pathogens, including the crucifer infecting TMV-Cg strain capable of compatible interactions with
365 the Arabidopsis UK-4 ecotype (Espinoza et al., 2007, Lim and Nam, 2005). Wound response,
366 mitotic cell arrest, and reduced photosynthetic efficiency are hallmarks for plant cell senescence
367 (Espinoza et al., 2007, Gan, 2003). Additionally, SA and JA, along with ET, contribute to
368 senescence in *Arabidopsis thaliana* (Schommer et al., 2008, Yu et al., 2021). Since all those
369 senescence hallmarks were present in our molecular characterization of the Marchantia-TMV
370 interaction, we first checked the expression levels of several senescence marker genes in our
371 transcriptomic data (Kulshrestha et al., 2022). We found that many senescence markers, such as
372 MpMYB14 (Mp5g19050), MpORE1 (Mp2g07720), MpNYE1 (Mp1g17090) and MpWRKY7
373 (Mp3g17660), were induced upon TMV infection, hence suggesting that TMV infection could
374 trigger aging and tissue maturation in Marchantia. Transcriptional trajectories orchestrating
375 maturation and aging in Marchantia, both at organism and tissue level, have been recently
376 reported to be very similar through transcriptional studies over developmental time, including
377 individuals from different ages (spanning from 1 day after germination - D1- to 31 days old
378 Marchantia plants -D31) , or by analysing sections along the thalli from top to base, being slice 1

379 (S1) at the top, considered the youngest part of the organ, and being slice 6 (S6) at the base and
380 considered the oldest (Wang et al., 2023). Thus, while S1 samples were more similar to D1, those
381 from S5 showed more commonalities to those from D31 plants. To assay whether TMV infection
382 could modify the life-history of Marchantia plants we compared the transcriptional profile
383 obtained from GFP positive areas from 4-week-old TMV-GFP infected Marchantia plants and that
384 from equivalent zones from mock treated individuals with those from the maturation and
385 developmental trajectories. Clustering of the transcriptional profile of mock and TMV infected
386 plants with those datasets, based on Pearson's correlation coefficient and regression model,
387 showed that TMV infection promotes maturation and aging. Thus, while the transcriptome from
388 mock treated plants clustered with juvenile state samples (slice 2 and Day 1), that from TMV
389 infected plants clustered with slice 4 and day 31 of development (Figure 5A, 5B).

390 Those results indicated that TMV infection triggers premature tissue maturation and senescence
391 in Marchantia, a characteristic trait from compatible plant - virus interactions.

392 **MpNAC7 is a conserved interactor of the TMV silencing suppressor p126 and enhances defense**
393 **against TMV in tobacco plants.**

394 The TMV replicase p126 is essential for viral replication and movement, but it also works as a
395 silencing suppressor in vascular plants (Ding et al., 2004). To gain insights into its possible role
396 during TMV infection in Marchantia plants, we first established its subcellular localization. We
397 found that p126 fused to GFP accumulated within the cytoplasm (Figure 6A) consistently with
398 earlier studies in onion epidermal cells, where the full length p126 protein fused to GFP was
399 found to be cytoplasmic (dos Reis Figueira et al., 2002).

400 Constitutive expression of viral-derived silencing suppressors often leads to plant developmental
401 defects, like growth stunting (Kasschau et al., 2003). Accordingly, four-weeks old Marchantia
402 plants constitutively expressing p126 were smaller in size when compared to control plants
403 (Figure 6B, Supplementary Fig. 9).

404 The TMV replicase p126 is known to associate with several host factors in Arabidopsis, including
405 TOM1 (Yamanaka et al., 2000), GDI2 (Kramer et al., 2011) and the transcription factor ATAF2
406 (Wang et al., 2009). To assess whether those interactions were conserved between p126 and the
407 corresponding orthologs in Marchantia, we performed Y2H assays. Orthologs were identified by
408 blasting the Arabidopsis protein sequences at MarpolBase (https//Marchantia.info) and
409 PlantRegMap (http://plantregmap.gao-lab.org/). The p126 full length and helicase domain

410 (Δp126, nt 2442 to 3636) were fused to the GAL4 binding domain and used as baits, while the
411 putative interactors fused to the GAL4-activation domain, were used as preys. Notably, the only
412 conserved interaction was that of the ortholog of the NAC transcription factor ATAF2, MpNAC7
413 (Mp6g02620), with Δp126 (Figure 6C). As for Δp126-ATAF2 binding (Wang et al., 2009) Δp126-
414 MpNAC7 interaction could be confirmed *in planta* using bimolecular luminescence
415 complementation (Figure 6D). Additionally, both the helicase domain alone and the full-length
416 p126 were found to interact *in planta* with either NAC transcription factors. Such discrepancy
417 between the results obtained by the two different protein-protein assays can be potentially
418 attributed to the presence of additional protein partners in Nicotiana or variable conditions ,
419 such as intracellular pH or growth temperature, that modify protein folding allowing the
420 interaction with the full length p126.

421 In Arabidopsis, ATAF2 expression is triggered by TMV infection (Wang et al., 2009). Likewise, we
422 found that MpNAC7 expression is also increased on TMV infection (Log2(fold-change)= 0.991),
423 wounding (Log2(fold-change)= 2.67), dn-OPDA and after 6 hours of SA treatment (Log2(fold-
424 change)= 1,23) in Marchantia. Likewise, ATAF2 is induced by wounding, SA and JA treatments
425 (Delessert et al., 2005) and contributes to defense against TMV in Arabidopsis (Wang et al.,
426 2009). Here, to ascertain the role of MpNAC7 in defense against TMV, and rule out a possible
427 link with RNA silencing- mediated responses, we infected 1 month old Nicotiana plants deficient
428 in RDR6 (rdr6i; (Schwach et al., 2005)) with MpNAC7, or GUS as control, in the presence of TMV
429 or an unrelated ssRNA virus, such as turnip mosaic virus (TuMV). TMV and TuMV strains were
430 labelled with the ROS1 gene which triggers anthocyanin production, and hence we followed
431 presence of the viruses by the purple colour (Bedoya et al., 2012). We observed that co-
432 expression of MpNAC7 abrogated local and systemic TMV infection with respect to plants co-
433 expressing the GUS control. By contrast, MpNAC7 co-expression was of no effect on TuMV
434 infected plants, that displayed a similar local and systemic presence of the virus as the GUS co-
435 infiltrated controls (Figure 6E, Supplementary Fig. 10).

436 Collectively, those results show that molecular interaction between the TMV silencing
437 suppressor p126 and the host NAC transcription factor is conserved in Marchantia, as well as the
438 role of this transcription factor in defense.

439 **Discussion**

440 In this work, we have characterized the interaction of the non-vascular liverwort *Marchantia*
441 *polymorpha* with viruses. First, we have defined known and unknown viruses that associate with
442 Marchantia. This showed that Marchantia is primarily associated with RNA viruses in nature,
443 validating previous predictions based on the presence of viral gene hallmarks in the
444 transcriptomes from the 1000 Plants Genome Project (Mushegian et al., 2016). We also showed
445 that at least one of these newly discovered viruses (Tübingen picorna-like virus 1) can replicate
446 in laboratory grown Marchantia Tak-1 plants. In-depth phylogenetic analyses placed this virus
447 within a larger, poorly characterised cluster composed of viruses discovered with metagenomics
448 approaches, mostly associated with environmental samples, within the *Picornavirales* order.
449 Viruses from this order infect mostly animals, but also protists and plants (Koonin et al., 2020)
450 Tübingen picorna-like virus 1 codes for the hallmark protein domains characteristic of
451 picornaviruses, but seems to lack movement protein (MP) that is present in most of the plant-
452 infecting viruses, with the exception of some vertically transmitted viruses, e.g., from families
453 *Paritiviridae* and *Amalgavirida (Dolja et al., 2020).*Although kinetics of viral replication is not
454 linear, in our infection experiment we observed only modest virus titre increase over time, which
455 might be connected to limited ability of the virus to move from cell-to-cell due to the lack of MP.
456 Few viruses have been identified by metagenomic approaches in non-vascular plants, such as *M.*
457 *polymorpha*, some with (Debat et al., 2023, Mifsud et al., 2022) and other without MP
458 (Mushegian et al., 2016, Vendrell-Mir et al., 2021). On the other hand, it is predicted that
459 plasmodesmata have evolved along with the acquisition of vasculature to assist in the transport
460 of nutrients throughout the plant by most likely changing the way they control their aperture
461 (Benitez et al., 2018, Hernandez-Hernandez et al., 2020). Therefore, it is plausible that the way
462 in which viruses interact with host plasmodesmata to move from cell-to-cell has also differed
463 over time. Additionally, it has also been recently proposed that viruses lacking a MP can
464 systemically infect vascular plants exploiting host proteins that are also present in Marchantia,
465 such as those belonging to the Phloem Protein 2 (PP2) gene family (Ying et al., 2024). Since we
466 only started to uncover the *M. polymorpha* virome, and, little is known about the structure and
467 function of *M. polymorpha* plasmodesmata (Zeinsmaster D.D and Carothers Z.B, 1974), involved
468 also in interaction with MP in vascular plants, further research building on the here developed
469 *M. polymorpha* inoculation procedures, will contribute to shed a light on the repertoire of viruses
470 infecting non-vascular plants. A recent study proposed a horizontal transfer of MP-encoding
471 viruses infecting vascular plants to non-vascular plants (Butkovic et al., 2023), whereas discovery
472 of Tübingen picorna-like virus 1 suggests another possible route of virus emergence in non-

473 vascular plants. This may be linked with horizontal virus transfer from invertebrates or protists
474 and could, very speculatively, represent a missing link in a recently suggested evolution of single
475 jelly roll type CP to MP (Butkovic et al., 2023).

476 Second, we have found that TMV engages into a compatible interaction with Marchantia plants.
477 That interaction encompasses an extensive transcriptional reprogramming reminiscent of that
478 found in vascular plants such as Arabidopsis and Nicotiana, albeit involving also previously
479 undescribed processes like the activation of a sustained wounding response here found in the
480 Marchantia-TMV interaction. Third, we have found that the TMV p126 silencing suppressor
481 displays similar subcellular localization in Marchantia cells, as in onion epidermal cells (dos Reis
482 Figueira et al., 2002), and that it interacts with MpNAC7, a NAC transcription factor ortholog of
483 the Arabidopsis ATAF2 factor involved in defense against TMV (Wang et al., 2009). Additionally,
484 transient expression of MpNAC7 specifically abrogates TMV infection in Nicotiana plants. All
485 those commonalities show that core molecular events of plant-virus interactions found in
486 vascular plants might be also present in non-vascular plants.

487 TMV infected Marchantia plants undergo a transcriptional reprogramming consistent with a
488 pathogenic process and characterized by the activation of defense related PR proteins and a
489 conserved PTI response. Perception of dsRNAs has been found to trigger PTI in response to TMV
490 infection in Arabidopsis, which in turn contributes to antiviral defense (Korner et al., 2013).
491 Indeed, dsRNA-triggered PTI is dependent on the Arabidopsis PRR co-receptor SERK1 (Niehl et
492 al., 2016), which has a corresponding ortholog in the Marchantia genome (Mp7g09160). This
493 very same Marchantia gene has been suggested as the ortholog of the Arabidopsis BAK1 gene,
494 which is central for PTI responses against *Pseudomonas syringae* (Gimenez-Ibanez, 2019).
495 Mp7g09160 has been shown to interact with the *P. syringae* effector AvrPto, which abrogates
496 PTI responses in Arabidopsis through interaction with AtBAK1 (Gimenez-Ibanez et al., 2019)..
497 Thus, it will be interesting in future studies to analyse the role of Mp7g09160 in viral PTI
498 responses. Additionally, TMV infection triggers the expression of a significant number of NLR
499 genes that can potentially contribute to an ETI response. While in *Nicotiana benthamiana*, both
500 DCL2 and DCL4 are processing TMV RNAs into 22 and 21 nucleotides long vsRNAs (Guo and
501 Wong, 2017), the solely presence of DCL4 in Marchantia results in a predominant processing in
502 21 nucleotides long vsRNAs. We also observed changes on the expression of core genes of the
503 RNA silencing machinery in response to TMV infection. In contrast to the repression of elements
504 from the RNA-Directed DNA methylation pathway, such as MpDCL3, MpAGO9 and MpNRPE1b,

505 the central elements within the RNA antiviral machinery MpDCL4 and MpRDR6 were activated.
506 Such general switch on RNA silencing pathways is reminiscent of that found in *Nicotiana*
507 *benthamiana* in response to TMV, although in *benthamiana* it is specifically restricted to the
508 vasculature (Collum and Culver, 2017). These results suggest an evolutionary re-routing of
509 defense mechanisms after acquisition of novel tissues or cell-types that become new focal points
510 for plant-virus interactions.

511 Interestingly, our results also uncover a previously unknown role of the wound response as an
512 antiviral defense mechanism. Plant cells undergoing wound responses experience inhibition of
513 their photosynthetic ability becoming sink tissues for photoassimilates (Quilliam et al., 2006),
514 attracting TMV movement (Brants, 1961). This wound response might be, at least partially,
515 sustained by the activation of the salicylic and jasmonate pathways. Thus, it is tempting to
516 speculate that sustained wound response in Marchantia plants, along with local and systemic
517 decreased on photosynthetic capability, confine TMV infection limiting its movement throughout
518 the plant. Additionally, premature senescence of infected tissues might further abrogate viral
519 infection. Therefore, modification of host´s life-history traits, such as senescence, can constitute
520 a defensive mechanism in Marchantia.

521 Salicylic and jasmonate pathways are central for defense against several pathogens. Although
522 the interaction between both hormones has been traditionally considered antagonistic, recent
523 studies suggest that such antagonism might have undergone evolutionary fine tuning, and hence
524 depend on each plant-microbe interaction (de Vries et al., 2018). Antagonism of the salicylic and
525 jasmonate pathways has been described in defense against bacterial and fungal pathogens in
526 Marchantia (Gimenez-Ibanez, 2019; Matsui, 2020). Our comparative analysis of the
527 transcriptional changes induced in response to TMV infection and those found in response to
528 treatments with Salicylic and jasmonates (dn-OPDA), or in Mpjaz-1 KO plants, show that both SA
529 and jasmonate pathways might contribute to the activation of genes involved in
530 phenylpropanoid metabolism. Those findings are in line with Salicylic and jasmonates triggering
531 this very same pathway in the moss *Physcomitrium patens,* which in turn is responsible for the
532 production of defense-related compounds. (de Vries et al., 2018). Likewise, in line with their
533 synergistic interaction being responsible for local and systemic resistance against TMV in
534 *Nicotiana benthamiana* (Zhu et al., 2014), both salicylic and jasmonates were observed to
535 activate genes involved in antiviral defense responses to TMV infection in Marchantia. Finally, a

536 set of SA/dn-OPDA commonly upregulated genes might contribute to the above mentioned
537 sustained wound response, and therefore, to contain virus spread.

538 Our work also highlights the conservation of central players, such as MpNAC7, in the specific
539 defense against TMV. Future comparative research studies will help to ascertain the conservation
540 of the genetic networks under MpNAC7 and ATAF2 regulation both in Marchantia and
541 Arabidopsis.

542 Collectively, results from this work suggest the presence of evolutionary conserved and divergent
543 plant strategies to cope with viral infections. Those might include gain and loss of defense
544 strategies, such as those involving wound responses. Evolution of plant-virus interactions might
545 also encompass the gradual acquisition of new elements within the underlying gene networks,
546 as those physically interacting with pathogen-derived proteins. Finally, defense mechanisms
547 might undergo anatomical re-location to newly pathogen-targeted cell-types and tissues over
548 evolutionary times.

549

550 **Methods**

551 Plant growth conditions

552 Male *Marchantia polymorpha* plants Takaragaike-1 (Tak-1) were grown on plates with half
553 strength Gamborg´s B5 medium (Duchefa) containing 1% agar and 1% sucrose under continuous
554 light and 22ºC.

555 *Nicotiana benthamiana* plants were grown on soil under long day conditions (16h light/ 8h dark)
556 and 25ºC.

557 Arabidopsis thaliana plants were grown on soil under long day conditions and 23 ºC.

558 Infection assays

559 Frozen tissue from Marchantia plants from the Tübingen population or lab grown Tak-1 plants
560 was homogenized in liquid nitrogen cold mortars, resuspended in phosphate buffer pH7.2,
561 filtered using 70 µM filters and kept at 4ºC. Two-week old Tak-1 plants grown in sterile conditions
562 in plates were vacuum incubated with each of both extracts and transferred to plates containing

563 wet soil. Eight Tak-1 individuals exposed to each sap were collected either one or two weeks
564 after incubation to assess viral replication.

565 Two week-old *Nicotiana benthamiana* plants were infiltrated with an agrobacterium solution
566 (0.5 O.D) carrying the TMV-GFP clone (Peart et al., 2002). Infected Nicotiana plants were grown
567 for 3 additional weeks along with non-infected plants and upper leaves displaying infection
568 symptoms were collected, along with equivalent ones from non-infected plants and frozen in
569 liquid nitrogen. Subsequently, leaf tissue was grinded in a liquid nitrogen cold mortar. Sap was
570 isolated from grinded leaf tissue using phosphate buffer pH 7.2, filtered with 70 µM filters and
571 maintained at 4ºC. Two-weeks old Tak-1 plants were incubated either in TMV-GFP containing sap
572 or sap from non-infected plants (mock) for 5 minutes in vacuum. After incubation, Tak-1 plants
573 were transferred to plates containing wet soil and brought back to the growth chamber. GFP
574 signal was monitored 1 and 2 weeks after incubation using a portable UV lamp or with a
575 magnifying stereoscope couple to a UV light source.

576 RNA isolation and expression analysis

577 Total RNA was extracted from Marchantia plants and Arabidopsis inflorescences using the
578 protocol described in (Box et al., 2011). Marchantia isolated RNA was further cleaned using the
579 RNeasy Kit (Qiagen). 500 ngs of total RNA were DNase I treated (Fisher Scientific) and converted
580 into cDNA using the RevertAid first strand kit (Fisher Scientific) following the manufacturer
581 instructions. RT-qPCR experiments were performed in a lightcycler (ROCHE) device. Relative
582 expression changes were calculated using the $2^{-\Delta\Delta Ct}$ method using *MpACTIN7* (Mp6g11010) gene
583 as housekeeping. Primers utilized can be found in supplementary table 3.

584 Samples for transcriptome assays were obtained from GFP positive areas collected from 5 4-
585 week-old Marchantia plants per replicate (4 replicates total) after two weeks incubation with
586 extracts from Nicotiana plants containing TMV-GFP. Equivalent areas were collected from mock
587 treated 4-week-old Marchantia plants as control. RNA was

588 RNA-seq analysis

589 For virome studies, 1 µg of total RNA from each of the 21 individuals included in the study was
590 pooled and 4 µg from the mixture were used for preparing two independent libraries using total
591 ribo-depleted RNA following the manufacturer instructions (Illumina TruSeq Stranded total RNA
592 LT sample prep Kit, plant). The first library containing samples from 14 individuals was sequenced

593 on an Illumina NovaSeq 6000 device in 2x150 bp mode, while the second one containing RNA
594 from 7 individuals, was sequenced in an Illumina NovaseqX device. A total of 306,895,552 and
595 506,670,250 reads were respectively obtained. The reads were trimmed and further analysed
596 using QIAGEN CLC Genomics Workbench 21 (https://digitalinsights.qiagen.com/). Dataset was
597 analysed for the presence of known and new viruses using an established virus detection
598 pipeline (Pecman et al., 2017), which includes: reads trimming, *de novo* assembly of trimmed
599 reads, mapping of reads and contigs to NCBI viral RefSeq database (search for known viruses)
600 and pFam domain search for contig sequences (search for known and unknown viruses). To
601 detect known viruses, results of reads mapping to viral RefSeq database were inspected and
602 filtered for viruses for which at least 1000 nts of the reference sequence were covered by
603 mapped reads (Supplementary Data 1). In parallel, to detect known viruses and search for new
604 ones, results of the pFam domain search of contig sequences were filtered for hits to viral
605 proteins. Then, this candidate list of viral contigs was additionally queried for similarity against
606 complete NCBI *nr* database (October 2020) using blastx (Gish and States, 1993) and the similarity
607 search results were visualized and taxonomically classified using MEGAN 6 (Huson et al., 2016).
608 Contigs corresponding to cellular organisms in this analysis were excluded from the list to obtain
609 a final list of putative viral-like sequences (Supplementary Data 2). Trimmed sequencing reads
610 were mapped to the list of putative viral-like sequences, to estimate the abundance of
611 corresponding nucleic acids in the sequenced sample and the results were reported as average
612 mapping depth (number of times a position is covered by sequencing reads, averaged over a
613 complete contig length; Supplementary Data 2).

614 The presence of selected viruses (three new and two known) was tested by RT-qPCR in RNA
615 extracts of collected samples as described above and datamining approach was used to search
616 for association of those viruses with different sample types linked with publicly available short
617 read datasets. This was performed by querying Serratus infrastructure palmprint database
618 (Edgar et al., 2022) by RdRp sequences of selected viruses using palmID tool
619 (https://serratus.io/palmid).

620 For a newly discovered picorna-like virus, named Tübingen picorna-like virus 1, additional
621 analyses were performed, aiming to ascertain its association with *M. polymorpha*. Putative
622 protein domains were annotated on the viral genome by InterProScan search
623 (https://www.ebi.ac.uk/interpro/search/sequence/, May 2024) of the two discovered open
624 reading frames against all included databases. Amino acid sequence of ORF 1 of the virus

625 (containing RNA-dependent polymerase (RdRp) domain) was queried for similarity against
626 complete NCBI *nr* database (January 2022) using blastp. Fifteen best hits according to bit score
627 values (which have at least 33% identity with the conserved part of the RdRp domain of the
628 queried virus) were included into phylogenetic analysis. Alignment of the sequences of the
629 conserved part of RdRp was performed using MAFFT 7.48 (Katoh and Standley, 2013), followed
630 by alignment trimming using TrimAI 1.3 in Automated 1 mode (Capella-Gutiérrez et al., 2009).
631 Then, best protein substitution model was selected using Model Finder (Kalyaanamoorthy et al.,
632 2017) and maximum likelihood phylogenetic tree inference was performed based on the
633 trimmed alignment using IQ-Tree 1.6.12 (Nguyen et al., 2015) using 1000 ultrafast bootstrap
634 replicates (Hoang et al., 2018). The resulting phylogenetic tree was visualized using iTOL 6.5
635 (Letunic and Bork, 2021) and viral taxa on the tree were coloured according to the associated
636 sample source, as designated in NCBI GenBank. To obtain even more in-depth information about
637 the phylogenetic position of the newly discovered virus, its sequence was aligned also against
638 members of the most related family-level cluster of RdRp sequences (f.0032) from RNA Viruses
639 in Metatranscriptomes (RVMT) database (https://riboviria.org/) (Neri et al., 2022). Alignment
640 and phylogenetic analyses were performed as described above, excluding TrimAI step.

641 For analysing the transcriptional response in Marchantia plants to TMV infection, 1 ug of total
642 RNA was used for preparing each stranded library by mRNA enrichment following manufacturer
643 indications (TrueSeq kit from Illumina). Libraries were sequenced on a Novaseq 6000 device. A
644 total of 20-21 million pairs were obtained per sample. Adapter removal and trimming of low
645 quality bases was done using Trim Galore! v0.6.1
646 (https://www.bioinformatics.babraham.ac.uk/projects/trim_galore/), removing reads shorter
647 than 20 bps and non-paired reads after the trimming step. Ribosomal RNA reads were removed
648 using SortMeRNA v2.1b (Kopylova et al., 2012), removing also reads that become unpaired after
649 this filtering step.

650 Cleaned reads together with the transcriptome of *Marchantia polymorpha* were used to quantify
651 gene expression at transcript level using Salmon v1.1.0 (Patro et al., 2017).

652 For this, the file MpTak1v5.1_r1.mrna.fasta containing the Marchantia transcriptome (v5.1) was
653 downloaded from https://marchantia.info/download/tak1v5.1/ (as of 19-Jan-2021). This file was
654 indexed using *Salmon index* and then used as input for *Salmon quant*, which was ran with
655 parameters -l A, –validateMappings, --recoverOrphans, --rangeFactorizationBins 4, --seqBias,
656 and –gcBias. Mapping rate was found to be in the 89.5%-92.58% range.

657 The R progam tximport v1.14.2 (Soneson et al., 2015) was used to aggregate Salmon's transcript
658 expression estimates at gene level and the *DESeqDataSetFromTximport* from the R package
659 DESeq2 v1.26.0 (Love et al., 2014) was used to create an R object with count data and
660 experimental information for all samples. A low-expression filter was then applied to remove any
661 gene with less than 10 counts across all 8 analyzed samples, resulting in a final set of 14,980
662 genes (from 19,217 annotated genes). Then, the *DESeq* function, which, among other things,
663 computes size factors for sample normalization, was applied to the filtered object. DESeq2's *rlog*
664 function was used to transform count data to the log2 scale while minimizing for differences
665 between samples for low-expressed genes. The transformed data was fed to DESeq2's *plotPCA*
666 function to visualize a PCA plot of the samples.

667 The analysis of differential expression was done using DESeq2's *results* function with the filtered
668 and normalized object as input and parameter *alpha = 0.05.*

669 All datasets used in this study for comparative analysis (wound response and salicylic acid time
670 course) were analysed in the very same way as described above.

671 All Gene ontology analysis (GO) were performed using PLAZA
672 (https://bioinformatics.psb.ugent.be/plaza/). Redundancy on representative categories was
673 reduced using Revigo (http://revigo.irb.hr/).

674 For correlation analysis of transcriptome responses between developmental trajectories and
675 TMV response, raw reads were processed as described above, except that rRNA was removed
676 using ribodetector_cpu v0.2.7 (Deng et al., 2022) and Salmon version was v1.9.0. Salmon's
677 counts were converted into a DESeq2 object and a low-expression filter was applied as described
678 above. Next, the existing batch effect between time course samples and sliced tissue ones was
679 removed using the Combat seq function from the sva package (Leek et al., 2023), v3.48.0. Then,
680 values for biological replicates were averaged and Pearson correlation was computed for the
681 resulting count matrix and displayed using the Heatmap function from the ComplexHeatmap
682 package (Gu, 2022). The batch correction, correlation and heatmap plotting steps were based
683 on the R script used in (Wang et al., 2023) and kindly provided by the authors.

684 DNA-seq data mining

685 Data mining was utilized to search for possible DNA viruses associated with *M. polymorpha.*
686 DNA-seq data from a recent study of *M. polymorpha* from natural populations (Beaulieu et al.,
687 2023) was retrieved from the SRA database (BioProject PRJNA931118). 74 biosample accessions

688 were selected to encompass diverse geographical locations and various *M. polymorpha*
689 subspecies. Datasets were analyzed using a customized pipeline for virus detection, designed
690 with the Snakemake workflow management system (v.7.32.4) (Köster et al., 2021). Some of the
691 chosen accessions contained sequencing data from multiple runs, which were merged before
692 analysis. The downloaded reads were processed using a custom script: (available at:
693 https://github.com/LanaVogrinec/snakemake-marchantia). Briefly, reads were trimmed with
694 trimmomatic (v.0.39) (Bolger et al., 2014) and assembled into contigs with MEGAHIT (v.1.2.9) (Li
695 et al., 2015). A similarity search was performed against the NCBI *nr* database (February 2024)
696 using DIAMOND (v.0.9.14) blastx (Buchfink et al., 2015) and the hits were taxonomically classified
697 with MEGAN6 (v.6.25.9) (Huson et al., 2016). Contig sequences classified as viral (group 'Viruses'
698 in MEGAN analysis) were extracted and are available, together with their classifications, in
699 Supplementary Data 6.

700 sRNA library construction and data processing

701 TMV-GFP positive areas were collected from 2 Marchantia plants infected for 2 weeks in two
702 biological replicates. RNA was isolated following the protocol described in (Box et al., 2011). 10
703 ngs of total RNA were used to build two independent libraries following manufacturer indications
704 (RealSeq-AC, Somagenics). Libraries were sequenced in an Illumina NovaSeq device. A total of
705 26-35 million single-end reads (101 bp) were obtained per sample. Adapter removal and
706 trimming of low quality bases was done using Trim Galore! v0.6.1
707 (https://www.bioinformatics.babraham.ac.uk/projects/trim_galore/) with parameters *-q 15 --*
708 *clip_R1 1 --length 16*.

709 Cleaned reads were then mapped to the TMV-GFP sequence using hisat2 (v2.1.0, (Kim et al.,
710 2019)) with default parameters. The resulting sam files were sorted and indexed using Samtools
711 (v1.15.1, (Danecek et al., 2021)) and the length distribution of reads mapping to the TMV-GFP
712 sequence was computed using samtools stats.

713 Constructs and plant transformation

714 cDNA from Marchantia mock treated plants was used to amplify the coding regions of *MpTOM1*
715 (Mp3g00660), *MpGDI2* (Mp6g05010) and *MpNAC7* (Mp6g02620) by PCR using Phusion
716 polymerase (NEB). Arabidopsis *Bobber1* (At5g53400) and *ATAF2* (At5g08790) were amplified
717 using cDNA synthesized from RNA from Arabidopsis inflorescences. p126 and Δp126 were
718 amplified using DNA from the TMV-GFP containing plasmid. All obtained fragments were further

719 incubated with dATP and Taq DNA polymerase (NEB) for 1 hour before cloned into the gateway
720 compatible vector PCR8/GW/TOPO TA (Invitrogen) or directly cloned to pENTR D-TOPO
721 (Invitrogen) in the case of ATAF2. An entry vector containing the Arabidopsis AGO1 was kindly
722 provided by Pablo Manavella. Inserts were cloned into their final vectors through LR reaction
723 using LR clonase II (Invitrogen). All plasmids were submitted to Sanger sequencing to corroborate
724 their integrity before used in the corresponding experiments. A list of primers used, and
725 constructs can be found in supplementary table 3 and supplementary table 4.

726 Plant transformation was performed as described in (Ishizaki et al., 2008) and selected in
727 Gamborg´s B5 media supplemented with Hygromycin 100mg/ml and Cefotaxime 100mg/ml.

728 Histology and imaging

729 Marchantia plants were embedded in 8% agarose and cross-sections of around 200 µM were
730 obtained using a vibratome. Confocal imaging was performed using Leica SP5. Images were
731 processed using Fiji (Schindelin et al., 2012).

732 Protein-protein interaction assays

733 Interactions in the yeast two-hybrid system were assayed on selective medium (L^-, W^-, H^-). The
734 assay was repeated 3 times. For the luciferase complementation assay, one-month old rdr6i
735 Nicotiana plants were used. *Agrobacterium tumefaciens* cultures with the different constructs
736 were mixed in the same amounts at a final OD_{600}=0.6. Leaves were imaged three days after
737 inoculation using a LAS4000 device. The assay was repeated 3 times with equivalent results.

738 Photosynthetic measurements

739 10 measurements per plant were performed in 5 infected and 5 mock treated individuals using
740 an IMAGING-PAM Maxi device (Heinz Walz GmbH). Quantification was done using the
741 ImagingWing integrated software.

742 Reporting summary

743 Further information on research design is available in the reporting summary linked to this
744 article.

745 **Data availability**

Raw data from the virome has been deposited in SRA and GenBank under Bioproject PRJNA1022866 (https://www.ncbi.nlm.nih.gov/bioproject/?term=PRJNA1022866) and BioSamples (SAMN37631837 and SAMN40978195). Raw data from TMV infected vs. Mock treated plants RNA-seq and TMV sRNA-seq have been deposit in SRA (Bioproject PRJNA1010197, https://www.ncbi.nlm.nih.gov/bioproject/?term=PRJNA1010197). Reconstructed genomic sequences of three novel viruses uncovered by virome analysis were deposited in NCBI GenBank (OR640980 https://www.ncbi.nlm.nih.gov/nuccore/OR640980, OR640981 https://www.ncbi.nlm.nih.gov/nuccore/OR640981, OR640982 https://www.ncbi.nlm.nih.gov/nuccore/OR640982). Raw data for other analysis included in this work can be found in the accompanying Source data file.

Code availability

Original code for DNA virome analysis can be accessed at https://github.com/LanaVogrinec/snakemake-marchantia, which has deposited at ZENODO under the ID 10.5281/zenodo.13359141 (https://zenodo.org/records/13359141).

References

BALLY, J., NAKASUGI, K., JIA, F., JUNG, H., HO, S. Y., WONG, M., PAUL, C. M., NAIM, F., WOOD, C. C., CROWHURST, R. N., HELLENS, R. P., DALE, J. L. & WATERHOUSE, P. M. 2015. The extremophile Nicotiana benthamiana has traded viral defence for early vigour. *Nat Plants,* 1**,** 15165.

BEAULIEU, C., LIBOUREL, C., MBADINGA ZAMAR, D. L., MAHBOUBI, K. E., HOEY, D. J., KELLER, J., GIROU, C., CLEMENTE, H. S., DIOP, I., AMBLARD, E., THÉRON, A., CAUET, S., RODDE, N., ZACHGO, S., HALPAPE, W., MEIERHENRICH, A., LAKER, B., BRAUTIGAM, A., GREIFF, G. R., SZOVENYI, P., CHENG, S., TANIZAWA, Y., LEEBENS-MACK, J. H., SCHMUTZ, J., WEBBER, J., GRIMWOOD, J., JACQUET, C., DUNAND, C., NELSON, J. M., ROUX, F., PHILIPPE, H., SCHORNACK, S., BONHOMME, M. & DELAUX, P.-M. 2023. The Marchantia pangenome reveals ancient mechanisms of plant adaptation to the environment. *bioRxiv***,** 2023.10.27.564390.

BECK, M., WYRSCH, I., STRUTT, J., WIMALASEKERA, R., WEBB, A., BOLLER, T. & ROBATZEK, S. 2014. Expression patterns of flagellin sensing 2 map to bacterial entry sites in plant shoots and roots. *J Exp Bot,* 65**,** 6487-98.

BEDOYA, L. C., MARTINEZ, F., ORZAEZ, D. & DAROS, J. A. 2012. Visual tracking of plant virus infection and movement using a reporter MYB transcription factor that activates anthocyanin biosynthesis. *Plant Physiol,* 158**,** 1130-8.

BELANGER, S., ZHAN, J. & MEYERS, B. C. 2023. Phylogenetic analyses of seven protein families refine the evolution of small RNA pathways in green plants. *Plant Physiol,* 192**,** 1183-1203.

783 BENITEZ, M., HERNANDEZ-HERNANDEZ, V., NEWMAN, S. A. & NIKLAS, K. J. 2018. Dynamical
784 Patterning Modules, Biogeneric Materials, and the Evolution of Multicellular Plants.
785 *Front Plant Sci,* 9**,** 871.
786 BOWLES, A. M. C., PAPS, J. & BECHTOLD, U. 2022. Water-related innovations in land plants
787 evolved by different patterns of gene cooption and novelty. *New Phytol,* 235**,** 732-742.
788 BOWMAN, J. L., KOHCHI, T., YAMATO, K. T., JENKINS, J., SHU, S., ISHIZAKI, K., YAMAOKA, S.,
789 NISHIHAMA, R., NAKAMURA, Y., BERGER, F., ADAM, C., AKI, S. S., ALTHOFF, F., ARAKI, T.,
790 ARTEAGA-VAZQUEZ, M. A., BALASUBRMANIAN, S., BARRY, K., BAUER, D., BOEHM, C. R.,
791 BRIGINSHAW, L., CABALLERO-PEREZ, J., CATARINO, B., CHEN, F., CHIYODA, S., CHOVATIA,
792 M., DAVIES, K. M., DELMANS, M., DEMURA, T., DIERSCHKE, T., DOLAN, L., DORANTES-
793 ACOSTA, A. E., EKLUND, D. M., FLORENT, S. N., FLORES-SANDOVAL, E., FUJIYAMA, A.,
794 FUKUZAWA, H., GALIK, B., GRIMANELLI, D., GRIMWOOD, J., GROSSNIKLAUS, U.,
795 HAMADA, T., HASELOFF, J., HETHERINGTON, A. J., HIGO, A., HIRAKAWA, Y., HUNDLEY, H.
796 N., IKEDA, Y., INOUE, K., INOUE, S. I., ISHIDA, S., JIA, Q., KAKITA, M., KANAZAWA, T.,
797 KAWAI, Y., KAWASHIMA, T., KENNEDY, M., KINOSE, K., KINOSHITA, T., KOHARA, Y., KOIDE,
798 E., KOMATSU, K., KOPISCHKE, S., KUBO, M., KYOZUKA, J., LAGERCRANTZ, U., LIN, S. S.,
799 LINDQUIST, E., LIPZEN, A. M., LU, C. W., DE LUNA, E., MARTIENSSEN, R. A., MINAMINO,
800 N., MIZUTANI, M., MIZUTANI, M., MOCHIZUKI, N., MONTE, I., MOSHER, R., NAGASAKI,
801 H., NAKAGAMI, H., NARAMOTO, S., NISHITANI, K., OHTANI, M., OKAMOTO, T.,
802 OKUMURA, M., PHILLIPS, J., POLLAK, B., REINDERS, A., ROVEKAMP, M., SANO, R., SAWA,
803 S., SCHMID, M. W., SHIRAKAWA, M., SOLANO, R., SPUNDE, A., SUETSUGU, N., SUGANO,
804 S., SUGIYAMA, A., SUN, R., SUZUKI, Y., TAKENAKA, M., et al. 2017. Insights into Land Plant
805 Evolution Garnered from the Marchantia polymorpha Genome. *Cell,* 171**,** 287-304 e15.
806 BOX, M. S., COUSTHAM, V., DEAN, C. & MYLNE, J. S. 2011. Protocol: A simple phenol-based
807 method for 96-well extraction of high quality RNA from Arabidopsis. *Plant Methods,* 7**,**
808 7.
809 BRANTS, D. H. 1961. The Influence of Meristematic Tissue and Injuries on the Transport of
810 Tobacco Mosaic Virus in Nicotiana tabacum L. cultivar. Samsun. *Acta Botanica*
811 *Neerlandica,* 10**,** 113-163.
812 BUTKOVIC, A., DOLJA, V. V., KOONIN, E. V. & KRUPOVIC, M. 2023. Plant virus movement proteins
813 originated from jelly-roll capsid proteins. *PLoS Biol,* 21**,** e3002157.
814 CAMPBELL, R. N. 1996. Fungal transmission of plant viruses. *Annu Rev Phytopathol,* 34**,** 87-108.
815 CAPELLA-GUTIÉRREZ, S., SILLA-MARTÍNEZ, J. M. & GABALDÓN, T. 2009. trimAl: a tool for
816 automated alignment trimming in large-scale phylogenetic analyses. *Bioinformatics,* 25**,**
817 1972-1973.
818 CARELLA, P., GOGLEVA, A., HOEY, D. J., BRIDGEN, A. J., STOLZE, S. C., NAKAGAMI, H. &
819 SCHORNACK, S. 2019. Conserved Biochemical Defenses Underpin Host Responses to
820 Oomycete Infection in an Early-Divergent Land Plant Lineage. *Curr Biol,* 29**,** 2282-2294
821 e5.
822 CARELLA, P., GOGLEVA, A., TOMASELLI, M., ALFS, C. & SCHORNACK, S. 2018. Phytophthora
823 palmivora establishes tissue-specific intracellular infection structures in the earliest
824 divergent land plant lineage. *Proc Natl Acad Sci U S A,* 115**,** E3846-E3855.
825 COLLUM, T. D. & CULVER, J. N. 2017. Tobacco mosaic virus infection disproportionately impacts
826 phloem associated translatomes in Arabidopsis thaliana and Nicotiana benthamiana.
827 *Virology,* 510**,** 76-89.
828 CHIA, K. S., KOURELIS, J., TEULET, A., VICKERS, M., SAKAI, T., WALKER, J. F., SCHORNACK, S.,
829 KAMOUN, S. & CARELLA, P. 2024a. The N-terminal domains of NLR immune receptors
830 exhibit structural and functional similarities across divergent plant lineages. *Plant Cell,*
831 36**,** 2491-2511.

832 CHIA, K. S., KOURELIS, J., TEULET, A., VICKERS, M., SAKAI, T., WALKER, J. F., SCHORNACK, S.,
833 KAMOUN, S. & CARELLA, P. 2024b. The N-terminal domains of NLR immune receptors
834 exhibit structural and functional similarities across divergent plant lineages. *Plant Cell*.
835 DANECEK, P., BONFIELD, J. K., LIDDLE, J., MARSHALL, J., OHAN, V., POLLARD, M. O., WHITWHAM,
836 A., KEANE, T., MCCARTHY, S. A., DAVIES, R. M. & LI, H. 2021. Twelve years of SAMtools
837 and BCFtools. *Gigascience,* 10.
838 DE VRIES, S., DE VRIES, J., VON DAHLEN, J. K., GOULD, S. B., ARCHIBALD, J. M., ROSE, L. E. &
839 SLAMOVITS, C. H. 2018. On plant defense signaling networks and early land plant
840 evolution. *Commun Integr Biol,* 11**,** 1-14.
841 DEBAT, H., GARCIA, M. L. & BEJERMAN, N. 2023. Expanding the Repertoire of the Plant-Infecting
842 Ophioviruses through Metatranscriptomics Data. *Viruses,* 15.
843 DELESSERT, C., KAZAN, K., WILSON, I. W., VAN DER STRAETEN, D., MANNERS, J., DENNIS, E. S. &
844 DOLFERUS, R. 2005. The transcription factor ATAF2 represses the expression of
845 pathogenesis-related genes in Arabidopsis. *Plant J,* 43**,** 745-57.
846 DENG, Z. L., MUNCH, P. C., MRECHES, R. & MCHARDY, A. C. 2022. Rapid and accurate
847 identification of ribosomal RNA sequences via deep learning. *Nucleic Acids Res,* 50**,** e60.
848 DING, S. W., HAN, Q., WANG, J. & LI, W. X. 2018. Antiviral RNA interference in mammals. *Curr*
849 *Opin Immunol,* 54**,** 109-114.
850 DING, S. W. & VOINNET, O. 2007. Antiviral immunity directed by small RNAs. *Cell,* 130**,** 413-26.
851 DING, X. S., LIU, J., CHENG, N. H., FOLIMONOV, A., HOU, Y. M., BAO, Y., KATAGI, C., CARTER, S. A.
852 & NELSON, R. S. 2004. The Tobacco mosaic virus 126-kDa protein associated with virus
853 replication and movement suppresses RNA silencing. *Mol Plant Microbe Interact,* 17**,**
854 583-92.
855 DOLJA, V. V., KRUPOVIC, M. & KOONIN, E. V. 2020. Deep Roots and Splendid Boughs of the Global
856 Plant Virome. *Annu Rev Phytopathol,* 58**,** 23-53.
857 DOS REIS FIGUEIRA, A., GOLEM, S., GOREGAOKER, S. P. & CULVER, J. N. 2002. A nuclear
858 localization signal and a membrane association domain contribute to the cellular
859 localization of the Tobacco mosaic virus 126-kDa replicase protein. *Virology,* 301**,** 81-9.
860 EDGAR, R. C., TAYLOR, B., LIN, V., ALTMAN, T., BARBERA, P., MELESHKO, D., LOHR, D.,
861 NOVAKOVSKY, G., BUCHFINK, B., AL-SHAYEB, B., BANFIELD, J. F., DE LA PENA, M.,
862 KOROBEYNIKOV, A., CHIKHI, R. & BABAIAN, A. 2022. Petabase-scale sequence alignment
863 catalyses viral discovery. *Nature,* 602**,** 142-147.
864 ERICKSON, F. L., HOLZBERG, S., CALDERON-URREA, A., HANDLEY, V., AXTELL, M., CORR, C. &
865 BAKER, B. 1999. The helicase domain of the TMV replicase proteins induces the N-
866 mediated defence response in tobacco. *Plant J,* 18**,** 67-75.
867 ESPINOZA, C., MEDINA, C., SOMERVILLE, S. & ARCE-JOHNSON, P. 2007. Senescence-associated
868 genes induced during compatible viral interactions with grapevine and Arabidopsis. *J Exp*
869 *Bot,* 58**,** 3197-212.
870 GAN, S. 2003. Mitotic and postmitotic senescence in plants. *Sci Aging Knowledge Environ,* 2003**,**
871 RE7.
872 GARCIA-RUIZ, H., TAKEDA, A., CHAPMAN, E. J., SULLIVAN, C. M., FAHLGREN, N., BREMPELIS, K. J.
873 & CARRINGTON, J. C. 2010. Arabidopsis RNA-dependent RNA polymerases and dicer-like
874 proteins in antiviral defense and small interfering RNA biogenesis during Turnip Mosaic
875 Virus infection. *Plant Cell,* 22**,** 481-96.
876 GIMENEZ-IBANEZ, S., ZAMARRENO, A. M., GARCIA-MINA, J. M. & SOLANO, R. 2019. An
877 Evolutionarily Ancient Immune System Governs the Interactions between Pseudomonas
878 syringae and an Early-Diverging Land Plant Lineage. *Curr Biol,* 29**,** 2270-2281 e4.
879 GISH, W. & STATES, D. J. 1993. Identification of protein coding regions by database similarity
880 search. *Nat Genet,* 3**,** 266-72.

881 GU, Z. 2022. Complex Heatmap Visualization. *iMeta*.
882 GUO, S. & WONG, S. M. 2017. Deep sequencing analysis reveals a TMV mutant with a poly(A)
883 tract reduces host defense responses in Nicotiana benthamiana. *Virus Res,* 239**,** 126-135.
884 HERNANDEZ-HERNANDEZ, V., BENITEZ, M. & BOUDAOUD, A. 2020. Interplay between turgor
885 pressure and plasmodesmata during plant development. *J Exp Bot,* 71**,** 768-777.
886 HEYMAN, J., CANHER, B., BISHT, A., CHRISTIAENS, F. & DE VEYLDER, L. 2018. Emerging role of the
887 plant ERF transcription factors in coordinating wound defense responses and repair. *J*
888 *Cell Sci,* 131.
889 HOANG, D. T., CHERNOMOR, O., VON HAESELER, A., MINH, B. Q. & VINH, L. S. 2018. UFBoot2:
890 Improving the Ultrafast Bootstrap Approximation. *Molecular Biology and Evolution,* 35**,**
891 518-522.
892 HUSON, D. H., BEIER, S., FLADE, I., GÓRSKA, A., EL-HADIDI, M., MITRA, S., RUSCHEWEYH, H. J. &
893 TAPPU, R. 2016. MEGAN Community Edition - Interactive Exploration and Analysis of
894 Large-Scale Microbiome Sequencing Data. *Plos Computational Biology,* 12.
895 ISHIZAKI, K., CHIYODA, S., YAMATO, K. T. & KOHCHI, T. 2008. Agrobacterium-mediated
896 transformation of the haploid liverwort Marchantia polymorpha L., an emerging model
897 for plant biology. *Plant Cell Physiol,* 49**,** 1084-91.
898 IWAMA, R. E. & MORAN, Y. 2023. Origins and diversification of animal innate immune responses
899 against viral infections. *Nat Ecol Evol,* 7**,** 182-193.
900 JEON, H.-W., IWAKAWA, H., MARAMOTO, S., HERRFURTH, C., GUSTCHE, N., SCHLÜTER, T.,
901 KYOZUKA, J., MIYAUCHI, S., FEUSSNER, I., ZACHGO, S. & NAKAGAMI, H. 2022. Contrasting
902 and conserved roles of NPR pathways in diverged land plant lineages. *bioRxiv*.
903 JIA, X., WANG, L., ZHAO, H., ZHANG, Y., CHEN, Z., XU, L. & YI, K. 2023. The origin and evolution of
904 salicylic acid signaling and biosynthesis in plants. *Mol Plant,* 16**,** 245-259.
905 KALYAANAMOORTHY, S., MINH, B. Q., WONG, T. K. F., VON HAESELER, A. & JERMIIN, L. S. 2017.
906 ModelFinder: fast model selection for accurate phylogenetic estimates. *Nature*
907 *Methods,* 14**,** 587-+.
908 KAPPAGANTU, M., COLLUM, T. D., DARDICK, C. & CULVER, J. N. 2020. Viral Hacks of the Plant
909 Vasculature: The Role of Phloem Alterations in Systemic Virus Infection. *Annu Rev Virol,*
910 7**,** 351-370.
911 KASSCHAU, K. D., XIE, Z., ALLEN, E., LLAVE, C., CHAPMAN, E. J., KRIZAN, K. A. & CARRINGTON, J.
912 C. 2003. P1/HC-Pro, a viral suppressor of RNA silencing, interferes with Arabidopsis
913 development and miRNA unction. *Dev Cell,* 4**,** 205-17.
914 KATOH, K. & STANDLEY, D. M. 2013. MAFFT Multiple Sequence Alignment Software Version 7:
915 Improvements in Performance and Usability. *Molecular Biology and Evolution,* 30**,** 772-
916 780.
917 KIM, D., PAGGI, J. M., PARK, C., BENNETT, C. & SALZBERG, S. L. 2019. Graph-based genome
918 alignment and genotyping with HISAT2 and HISAT-genotype. *Nat Biotechnol,* 37**,** 907-
919 915.
920 KNEESHAW, S., SORIANO, G., MONTE, I., HAMBERG, M., ZAMARRENO, A. M., GARCIA-MINA, J.
921 M., FRANCO-ZORRILLA, J. M., KATO, N., UEDA, M., REY-STOLLE, M. F., BARBAS, C.,
922 MICHAVILA, S., GIMENEZ-IBANEZ, S., JIMENEZ-ALEMAN, G. H. & SOLANO, R. 2022.
923 Ligand diversity contributes to the full activation of the jasmonate pathway in
924 Marchantia polymorpha. *Proc Natl Acad Sci U S A,* 119**,** e2202930119.
925 KOONIN, E. V., DOLJA, V. V., KRUPOVIC, M., VARSANI, A., WOLF, Y. I., YUTIN, N., ZERBINI, F. M. &
926 KUHN, J. H. 2020. Global Organization and Proposed Megataxonomy of the Virus World.
927 *Microbiol Mol Biol Rev,* 84.
928 KOPYLOVA, E., NOÉ, L. & TOUZET, H. 2012. SortMeRNA: fast and accurate filtering of ribosomal
929 RNAs in metatranscriptomic data. *Bioinformatics,* 28**,** 3211-3217.

930 KORNER, C. J., KLAUSER, D., NIEHL, A., DOMINGUEZ-FERRERAS, A., CHINCHILLA, D., BOLLER, T.,
931 HEINLEIN, M. & HANN, D. R. 2013. The immunity regulator BAK1 contributes to
932 resistance against diverse RNA viruses. *Mol Plant Microbe Interact,* 26**,** 1271-80.
933 KRAMER, S. R., GOREGAOKER, S. P. & CULVER, J. N. 2011. Association of the Tobacco mosaic virus
934 126kDa replication protein with a GDI protein affects host susceptibility. *Virology,* 414**,**
935 110-8.
936 KULSHRESTHA, S., JIBRAN, R., VAN KLINK, J. W., ZHOU, Y., BRUMMELL, D. A., ALBERT, N. W.,
937 SCHWINN, K. E., CHAGNE, D., LANDI, M., BOWMAN, J. L. & DAVIES, K. M. 2022. Stress,
938 senescence, and specialized metabolites in bryophytes. *J Exp Bot,* 73**,** 4396-4411.
939 LEE, W. S., FU, S. F., LI, Z., MURPHY, A. M., DOBSON, E. A., GARLAND, L., CHALUVADI, S. R., LEWSEY,
940 M. G., NELSON, R. S. & CARR, J. P. 2016. Salicylic acid treatment and expression of an
941 RNA-dependent RNA polymerase 1 transgene inhibit lethal symptoms and meristem
942 invasion during tobacco mosaic virus infection in Nicotiana benthamiana. *BMC Plant*
943 *Biol,* 16**,** 15.
944 LEEK, J. T., JOHNSON, W. E., PARKER, H. S., FERTIG, E. J., JAFFE, A.E., ZHANG, Y., STOREY, J. D. &
945 TORRES, L. C. 2023. sva: Surrogate Variable Analysis.
946 LETUNIC, I. & BORK, P. 2021. Interactive Tree Of Life (iTOL) v5: an online tool for phylogenetic
947 tree display and annotation. *Nucleic Acids Research,* 49**,** W293-W296.
948 LEWSEY, M. G. & CARR, J. P. 2009. Effects of DICER-like proteins 2, 3 and 4 on cucumber mosaic
949 virus and tobacco mosaic virus infections in salicylic acid-treated plants. *J Gen Virol,* 90**,**
950 3010-3014.
951 LIANG, Y., HEYMAN, J., XIANG, Y., VANDENDRIESSCHE, W., CANHER, B., GOEMINNE, G. & DE
952 VEYLDER, L. 2022. The wound-activated ERF15 transcription factor drives Marchantia
953 polymorpha regeneration by activating an oxylipin biosynthesis feedback loop. *Sci Adv,*
954 8**,** eabo7737.
955 LIM, P. O. & NAM, H. G. 2005. The molecular and genetic control of leaf senescence and longevity
956 in Arabidopsis. *Curr Top Dev Biol,* 67**,** 49-83.
957 LIU, C. & NELSON, R. S. 2013. The cell biology of Tobacco mosaic virus replication and movement.
958 *Front Plant Sci,* 4**,** 12.
959 LIU, Y., GAO, Q., WU, B., AI, T. & GUO, X. 2009. NgRDR1, an RNA-dependent RNA polymerase
960 isolated from Nicotiana glutinosa, was involved in biotic and abiotic stresses. *Plant*
961 *Physiol Biochem,* 47**,** 359-68.
962 LOPEZ-GOMOLLON, S. & BAULCOMBE, D. C. 2022. Roles of RNA silencing in viral and non-viral
963 plant immunity and in the crosstalk between disease resistance systems. *Nat Rev Mol*
964 *Cell Biol,* 23**,** 645-662.
965 LOVE, M. I., HUBER, W. & ANDERS, S. 2014. Moderated estimation of fold change and dispersion
966 for RNA-seq data with DESeq2. *Genome Biol,* 15**,** 550.
967 LUCAS, W. J., GROOVER, A., LICHTENBERGER, R., FURUTA, K., YADAV, S. R., HELARIUTTA, Y., HE, X.
968 Q., FUKUDA, H., KANG, J., BRADY, S. M., PATRICK, J. W., SPERRY, J., YOSHIDA, A., LOPEZ-
969 MILLAN, A. F., GRUSAK, M. A. & KACHROO, P. 2013. The plant vascular system: evolution,
970 development and functions. *J Integr Plant Biol,* 55**,** 294-388.
971 MANDADI, K. K. & SCHOLTHOF, K. B. 2013. Plant immune responses against viruses: how does a
972 virus cause disease? *Plant Cell,* 25**,** 1489-505.
973 MATSUI, H., IWAKAWA, H., HYON, G. S., YOTSUI, I., KATOU, S., MONTE, I., NISHIHAMA, R.,
974 FRANZEN, R., SOLANO, R. & NAKAGAMI, H. 2020. Isolation of Natural Fungal Pathogens
975 from Marchantia polymorpha Reveals Antagonism between Salicylic Acid and Jasmonate
976 during Liverwort-Fungus Interactions. *Plant Cell Physiol,* 61**,** 265-275.

977 MIFSUD, J. C. O., GALLAGHER, R. V., HOLMES, E. C. & GEOGHEGAN, J. L. 2022. Transcriptome
978 Mining Expands Knowledge of RNA Viruses across the Plant Kingdom. *J Virol,* 96**,**
979 e0026022.
980 MONTE, I., FRANCO-ZORRILLA, J. M., GARCIA-CASADO, G., ZAMARRENO, A. M., GARCIA-MINA, J.
981 M., NISHIHAMA, R., KOHCHI, T. & SOLANO, R. 2019. A Single JAZ Repressor Controls the
982 Jasmonate Pathway in Marchantia polymorpha. *Mol Plant,* 12**,** 185-198.
983 MONTE, I., ISHIDA, S., ZAMARRENO, A. M., HAMBERG, M., FRANCO-ZORRILLA, J. M., GARCIA-
984 CASADO, G., GOUHIER-DARIMONT, C., REYMOND, P., TAKAHASHI, K., GARCIA-MINA, J.
985 M., NISHIHAMA, R., KOHCHI, T. & SOLANO, R. 2018. Ligand-receptor co-evolution shaped
986 the jasmonate pathway in land plants. *Nat Chem Biol,* 14**,** 480-488.
987 MUSHEGIAN, A., SHIPUNOV, A. & ELENA, S. F. 2016. Changes in the composition of the RNA
988 virome mark evolutionary transitions in green plants. *BMC Biol,* 14**,** 68.
989 NERI, U., WOLF, Y. I., ROUX, S., CAMARGO, A. P., LEE, B., KAZLAUSKAS, D., CHEN, I. M., IVANOVA,
990 N., ZEIGLER ALLEN, L., PAEZ-ESPINO, D., BRYANT, D. A., BHAYA, D., CONSORTIUM, R. N. A.
991 V. D., KRUPOVIC, M., DOLJA, V. V., KYRPIDES, N. C., KOONIN, E. V. & GOPHNA, U. 2022.
992 Expansion of the global RNA virome reveals diverse clades of bacteriophages. *Cell,* 185**,**
993 4023-4037 e18.
994 NGUYEN, L. T., SCHMIDT, H. A., VON HAESELER, A. & MINH, B. Q. 2015. IQ-TREE: A Fast and
995 Effective Stochastic Algorithm for Estimating Maximum-Likelihood Phylogenies.
996 *Molecular Biology and Evolution,* 32**,** 268-274.
997 NIEHL, A., WYRSCH, I., BOLLER, T. & HEINLEIN, M. 2016. Double-stranded RNAs induce a pattern-
998 triggered immune signaling pathway in plants. *New Phytol,* 211**,** 1008-19.
999 PAGAN, I., ALONSO-BLANCO, C. & GARCIA-ARENAL, F. 2008. Host responses in life-history traits
1000 and tolerance to virus infection in Arabidopsis thaliana. *PLoS Pathog,* 4**,** e1000124.
1001 PATRO, R., DUGGAL, G., LOVE, M. I., IRIZARRY, R. A. & KINGSFORD, C. 2017. Salmon provides fast
1002 and bias-aware quantification of transcript expression. *Nature Methods,* 14**,** 417-+.
1003 PEART, J. R., COOK, G., FEYS, B. J., PARKER, J. E. & BAULCOMBE, D. C. 2002. An EDS1 orthologue
1004 is required for N-mediated resistance against tobacco mosaic virus. *Plant J,* 29**,** 569-79.
1005 PRUITT, R. N., LOCCI, F., WANKE, F., ZHANG, L., SAILE, S. C., JOE, A., KARELINA, D., HUA, C.,
1006 FROHLICH, K., WAN, W. L., HU, M., RAO, S., STOLZE, S. C., HARZEN, A., GUST, A. A.,
1007 HARTER, K., JOOSTEN, M., THOMMA, B., ZHOU, J. M., DANGL, J. L., WEIGEL, D.,
1008 NAKAGAMI, H., OECKING, C., KASMI, F. E., PARKER, J. E. & NURNBERGER, T. 2021. The
1009 EDS1-PAD4-ADR1 node mediates Arabidopsis pattern-triggered immunity. *Nature,* 598**,**
1010 495-499.
1011 QUILLIAM, R. S., SWARBRICK, P. J., SCHOLES, J. D. & ROLFE, S. A. 2006. Imaging photosynthesis in
1012 wounded leaves of Arabidopsis thaliana. *J Exp Bot,* 57**,** 55-69.
1013 RAKHSHANDEHROO, F., REZAEE, S. & PALUKAITIS, P. 2017. Silencing the tobacco gene for RNA-
1014 dependent RNA polymerase 1 and infection by potato virus Y cause remodeling of
1015 cellular organelles. *Virology,* 510**,** 127-136.
1016 REDKAR, A., GIMENEZ IBANEZ, S., SABALE, M., ZECHMANN, B., SOLANO, R. & DI PIETRO, A. 2022.
1017 Marchantia polymorpha model reveals conserved infection mechanisms in the vascular
1018 wilt fungal pathogen Fusarium oxysporum. *New Phytol,* 234**,** 227-241.
1019 SCHINDELIN, J., ARGANDA-CARRERAS, I., FRISE, E., KAYNIG, V., LONGAIR, M., PIETZSCH, T.,
1020 PREIBISCH, S., RUEDEN, C., SAALFELD, S., SCHMID, B., TINEVEZ, J. Y., WHITE, D. J.,
1021 HARTENSTEIN, V., ELICEIRI, K., TOMANCAK, P. & CARDONA, A. 2012. Fiji: an open-source
1022 platform for biological-image analysis. *Nat Methods,* 9**,** 676-82.
1023 SCHOLTHOF, K. B. 2004. Tobacco mosaic virus: a model system for plant biology. *Annu Rev*
1024 *Phytopathol,* 42**,** 13-34.

1025 SCHOMMER, C., PALATNIK, J. F., AGGARWAL, P., CHETELAT, A., CUBAS, P., FARMER, E. E., NATH,
1026 U. & WEIGEL, D. 2008. Control of jasmonate biosynthesis and senescence by miR319
1027 targets. *PLoS Biol,* 6**,** e230.
1028 SCHWACH, F., VAISTIJ, F. E., JONES, L. & BAULCOMBE, D. C. 2005. An RNA-dependent RNA
1029 polymerase prevents meristem invasion by potato virus X and is required for the activity
1030 but not the production of a systemic silencing signal. *Plant Physiol,* 138**,** 1842-52.
1031 SHENG, Y., YANG, L., LI, C., WANG, Y. & GUO, H. 2019. Transcriptomic changes in Nicotiana
1032 tabacum leaves during mosaic virus infection. *3 Biotech,* 9**,** 220.
1033 SIEVERT, R.C.. 1978. Effect of Potato Virus Y and Tobacco Mosaic Virus on Field-Grown Burley
1034 Tobacco. *PHYTOPATHOLOGY,* 68**,** 823-825.
1035 SILVESTRI, A., BANSAL, C. & RUBIO-SOMOZA, I. 2024. After silencing suppression: miRNA targets
1036 strike back. *Trends Plant Sci*.
1037 SONESON, C., LOVE, M. I. & ROBINSON, M. D. 2015. Differential analyses for RNA-seq: transcript-
1038 level estimates improve gene-level inferences. *F1000Res,* 4**,** 1521.
1039 VASSEUR, F., BALDRICH, P., JIMENEZ-GONGORA, T., VILLAR-MARTIN, L., WEIGEL, D. & RUBIO-
1040 SOMOZA, I. 2022. miRNA472 deficiency enhances Arabidopsis thaliana defence without
1041 reducing seed production. *bioRxiv,* doi.org/10.1101/2022.12.13.520224
1042 VENDRELL-MIR, P., PERROUD, P. F., HAAS, F. B., MEYBERG, R., CHARLOT, F., RENSING, S. A.,
1043 NOGUE, F. & CASACUBERTA, J. M. 2021. A vertically transmitted amalgavirus is present
1044 in certain accessions of the bryophyte Physcomitrium patens. *Plant J,* 108**,** 1786-1797.
1045 WANG, L., WAN, M. C., LIAO, R. Y., XU, J., XU, Z. G., XUE, H. C., MAI, Y. X. & WANG, J. W. 2023. The
1046 maturation and aging trajectory of Marchantia polymorpha at single-cell resolution. *Dev*
1047 *Cell,* 58**,** 1429-1444 e6.
1048 WANG, X., GOREGAOKER, S. P. & CULVER, J. N. 2009. Interaction of the Tobacco mosaic virus
1049 replicase protein with a NAC domain transcription factor is associated with the
1050 suppression of systemic host defenses. *J Virol,* 83**,** 9720-30.
1051 WHITHAM, S., DINESH-KUMAR, S. P., CHOI, D., HEHL, R., CORR, C. & BAKER, B. 1994. The product
1052 of the tobacco mosaic virus resistance gene N: similarity to toll and the interleukin-1
1053 receptor. *Cell,* 78**,** 1101-15.
1054 XU, T., ZHANG, L., ZHEN, J., FAN, Y., ZHANG, C. & WANG, L. 2013. Expressional and regulatory
1055 characterization of Arabidopsis RNA-dependent RNA polymerase 1. *Planta,* 237**,** 1561-9.
1056 XU, X. J., GENG, C., JIANG, S. Y., ZHU, Q., YAN, Z. Y., TIAN, Y. P. & LI, X. D. 2022. A maize
1057 triacylglycerol lipase inhibits sugarcane mosaic virus infection. *Plant Physiol,* 189**,** 754-
1058 771.
1059 YAMANAKA, T., OHTA, T., TAKAHASHI, M., MESHI, T., SCHMIDT, R., DEAN, C., NAITO, S. &
1060 ISHIKAWA, M. 2000. TOM1, an Arabidopsis gene required for efficient multiplication of
1061 a tobamovirus, encodes a putative transmembrane protein. *Proc Natl Acad Sci U S A,* 97**,**
1062 10107-12.
1063 YING, X. B., DONG, L., ZHU, H., DUAN, C. G., DU, Q. S., LV, D. Q., FANG, Y. Y., GARCIA, J. A., FANG,
1064 R. X. & GUO, H. S. 2010. RNA-dependent RNA polymerase 1 from Nicotiana tabacum
1065 suppresses RNA silencing and enhances viral infection in Nicotiana benthamiana. *Plant*
1066 *Cell,* 22**,** 1358-72.
1067 YOTSUI, I., MATSUI, H., MIYAUCHI, S., IWAKAWA, H., MELKONIAN, K., SCHLUTER, T., MICHAVILA,
1068 S., KANAZAWA, T., NOMURA, Y., STOLZE, S. C., JEON, H. W., YAN, Y., HARZEN, A., SUGANO,
1069 S. S., SHIRAKAWA, M., NISHIHAMA, R., ICHIHASHI, Y., IBANEZ, S. G., SHIRASU, K., UEDA,
1070 T., KOHCHI, T. & NAKAGAMI, H. 2023. LysM-mediated signaling in Marchantia
1071 polymorpha highlights the conservation of pattern-triggered immunity in land plants.
1072 *Curr Biol,* 33**,** 3732-3746 e8.

YU, D., FAN, B., MACFARLANE, S. A. & CHEN, Z. 2003. Analysis of the involvement of an inducible Arabidopsis RNA-dependent RNA polymerase in antiviral defense. *Mol Plant Microbe Interact,* 16**,** 206-16.

YU, X., XU, Y. & YAN, S. 2021. Salicylic acid and ethylene coordinately promote leaf senescence. *J Integr Plant Biol,* 63**,** 823-827.

ZAMFIR, A. D., BABALOLA, B. M., FRAILE, A., MCLEISH, M. J. & GARCIA-ARENAL, F. 2023. Tobamoviruses Show Broad Host Ranges and Little Genetic Diversity Among Four Habitat Types of a Heterogeneous Ecosystem. *Phytopathology,* 113**,** 1697-1707.

ZEINSMASTER D.D & CAROTHERS Z.B 1974. The Fine Structure of Oogenesis in Marchantia polymorpha. *American Journal of Botany,* 61**,** 499-512.

ZHU, F., XI, D. H., YUAN, S., XU, F., ZHANG, D. W. & LIN, H. H. 2014. Salicylic acid and jasmonic acid are essential for systemic resistance against tobacco mosaic virus in Nicotiana benthamiana. *Mol Plant Microbe Interact,* 27**,** 567-77.

Acknowledgments

We would like to thank Juan Jose López-Moya, Miguel A. Blázquez and Salomé Prat for critical reading of the manuscript. Sebastian Schornack, Phil Carella, Alexander Summers, the CUBG curation team (Samuel Brockington and Mar Millan), Klaus Schlaeppi, Katja Rembold, Alba Gonzalez, Detlef Weigel, Alexandra Kehl, Brigitte Fiebig, Luisa Lanfranco, Mara Novero, Isabel Monte, Adrián Vojtassák, Sabine Zachgo and Claudia Gieshoidt for their help in obtaining Marchantia individuals for the virome assays. Neža Pajek Arambašić for help with pipeline automation. We would like to thank Eduardo Bejarano for providing the plasmid containing TMV-GFP and Antonio Darós for providing TuMV-ROS1 and TMV-ROS1 containing plasmids. Pablo Manavella for the AtAGO1-pEntr plasmid. Phil Carella for an updated annotation of NLR genes in Marchantia. We would also thank to Jia-Wei Wang, Long Wang and Jie Xu for sharing the code used for correlation analysis between TMV transcriptional responses and the different samples from Marchantia developmental trajectories.

The work in the MoRE lab is funded by RYC-2015-19154 (funded by MCIN/AEI/ 10.13039/501100011033 and by “ESF Investing in your future”), RTI2018-097262-B-I00 (funded by MCIN/AEI/ 10.13039/501100011033 and by “ERDF A way of making Europe”) and through the “Severo Ochoa Programme for Centres of Excellence in R&D” 2016-2019 (SEV-2015-0533) and 2020-2023 (CEX2019-000902-S) funded by MCIN/AEI/ 10.13039/501100011033,CSIC-MCIN (Grant 202240I201) and the CERCA and SGR (2021-SGR-00875) programmes from the Generalitat de Catalunya to I-R-S. T J-G was recipient of a Postdoctoral Fellowship from CRAG through the “Severo Ochoa Programme for Centres of Excellence in R&D” 2016-2019 (SEV-2015-0533). L. V-M was supported by BES-2016-076986 (funded by MCIN/AEI/ 10.13039/501100011033 and by “ESF Investing in your future”). The work at NIB was funded by

1109 Slovenian Research and Innovation Agency core and project financing P4-0407, P4-0165 and J4-
1110 4553.

1111 Authors contributions

1112 I.R-S. and T.J-G. conceptualized the study and designed experiments. I.R-S. supervised the study
1113 and acquired funding. T.J-G. and I.R-S. isolated RNAs for virome analysis. D.K. and L.V. performed
1114 virome analysis. E.R-M. and L.V-M. performed expression analysis of presence of viruses in
1115 natural Marchantia populations and Marchantia infection with natural viruses. T.J-G. and I.R-S.
1116 performed histological and expression analysis of viral infections. I.R-S. and V.M.G-M. performed
1117 RNA isolation, sRNA libraries and analysis for transcriptomic assays. E.R-M. carried out all
1118 phenotypic and p126 histological studies. I.R-S. carried out the protein-protein interaction assays
1119 and performed infection assays in Nicotiana. I.R-S. and D.K. wrote the manuscript with input
1120 from all authors.
1121

1122 Corresponding author
1123 Correspondence to ignacio.rubio@cragenomica.es
1124

1125 **Ethics declarations**

1126 Competing interests

1127 The authors declare no competing interests

1128 **Figure legends**

1129 **Figure 1.** Marchantia polymorpha is infected by RNA viruses.

1130 (A) Genome structure of Tübingen picorna-like virus 1, newly discovered in composite *M.*
1131 *polymorpha* sample with two predicted open reading frames (ORFs) and corresponding
1132 average reads mapping depth in sequenced composite sample. Black empty boxes
1133 represent predicted protein domains detected by InterProScan: S3H – superfamily 3
1134 helicase, 3C-Pro – peptidase C3, RdRp – RNA-dependent RNA polymerase and CP-SJR – coat
1135 protein with 8-stranded jelly roll β-barrel motif.

1136 (B) Maximum likelihood phylogenetic tree obtained based on the alignment of the
1137 conserved part of RdRd of Tübingen picorna-like virus 1 and fifteen other most similar
1138 viruses. The tree was midpoint rooted. Coloured virus names correspond to the sources

1139 associated with a particular virus, according to the legend on the right side of the panel.
1140 Numbers next to the branches represent statistical support (%) of the clades according to
1141 the ultrafast bootstrap analysis. Branch length represents the average number of amino acid
1142 substitutions per site. Codes next to the taxon names in round brackets are the
1143 corresponding NCBI GenBank protein accession numbers. Next to them, fractions in square
1144 brackets represent % of identity of Tübingen picorna-like virus 1 to other individual taxons
1145 for the aligned part of the RdRp domain.

1146 (C) Results of the viral concentration measurements for *M. polymorpha* plants inoculated
1147 with Tübingen picorna-like virus 1 positive plant extracts. On the right, relative
1148 concentrations of Tübingen picorna-like virus 1 in inoculated plants one- and two-weeks
1149 post inoculation are shown; measurements of concentrations in individual plants (from 3
1150 technical replicates each) are shown as dots (n=8 for both time points) and the box-whisker
1151 plots represent the distribution of values (showing median as a thick line, first and third
1152 quartile as boxes and minimum and maximum as whiskers) for the two time points (at 1
1153 WPI, x represent an outlier measurement). On the top of the plot, the horizontal connecting
1154 line designates statistically significant difference in the means of the two distributions, with
1155 the corresponding p-value, according to the nonparametric Wilcoxon rank sum test (two-
1156 sided). Source data are provided as a Source data File. BIORENDER was used to prepare this
1157 figure.

1158 **Figure 2**. Tobacco mosaic virus replicates in Marchantia plants.

1159 (A) GFP fluorescent signal (in yellow) increases in thalli from 3-week-old plants after 1 week,
1160 (left panel) compared to thalli from 4 weeks old and 2-weeks infected plants (right
1161 panel). Both images show the same part or an infected plant under a magnification
1162 device under UV light. Magenta shows chlorophyll autofluorescence. White bar scale
1163 shows 100 µms. This experiment was repeated 4 times, and one additional replicate is
1164 shown in Supplementary Fig. 3.
1165 (B) TMV-GFP transcripts increase over time in infected plants. Pools of three infected plants
1166 were used for each time point. The result from 3 technical replicates is shown, with two
1167 complementary replicates showing the same trend in Supplementary Fig. 4. Mock, 4
1168 weeks old plants incubated with sap from untreated plants. T0, 2 weeks old plants
1169 collected right after incubation with sap from infected plants. T1, 3 weeks old plants
1170 collected after 1 week from incubation. T2, 4 weeks old plants collected after 3 weeks

1171 from incubation. Expression of TMV is relative to the expression of Marchantia actine.
1172 Source data are provided as a Source data File.
1173 (C) Length distribution of TMV-derived vsRNAs populations found in thalli from 4 weeks old
1174 plants after 2 weeks of infection. Nts stans for nucleotides.
1175 (D) TMV-GFP infects all cell types. Transversal sections of an Marchantia thalli from a mock
1176 treated plant that was 4 weeks old (left) and equivalent area in a plant 2 weeks after
1177 infection (right) under confocal image. The pictures show the merge between green (in
1178 yellow, GFP-labelled virus) and red (in magenta, autofluorescence) channels. Merge was
1179 performed using Fiji. P stands for Photosynthetic region, S for storage region and E stands
1180 for lower epidermis. White bar scale shows 100 µm. This experiment was repeated 3
1181 times showing similar results.

1182 **Figure 3.** TMV triggers stress-related molecular reprogramming in Marchantia.

1183 (A) Set of common PTI marker genes responsive to bacterial and fungal extracts and TMV in
1184 infected areas in thalli from 4 weeks old plants after 2 weeks of infection compared to
1185 equivalent areas from mock treated plants. DESeq2 results using the default parameters
1186 (Wald test and Benjamini-Hochberg p adjustment method)
1187 (B) Set of wound and TMV responsive ERF transcription factors. DESeq2 results using the
1188 default parameters (Wald test and Benjamini-Hochberg p adjustment method)
1189 (C) Venn diagram showing that transcriptional reprogramming upon TMV infection largely
1190 overlaps with that found upon wounding.
1191 (D) Set of chitin and TMV responsive WRKY transcription factors in Marchantia. DESeq2
1192 results using the default parameters (Wald test and Benjamini-Hochberg p adjustment
1193 method)
1194 (E) Photosynthetic efficiency (Fv/Fm) in infected areas in thalli from 4 weeks old plants after
1195 2 weeks of infection compared to equivalent areas from mock treated plants. 5 biological
1196 and 10 technical replicates for each were assayed in both infected and mock treated
1197 plants. Statistical assessment was performed using a two-sided parametric T-test. Length
1198 of the whiskers: 1.5 x IQR. Central line: median. Box width: IQR (i.e. Q3-Q1). Source data
1199 are provided as a Source data File. Marchantia plants and cameras depicting measured
1200 areas come from Biorender. Light green area indicated TMV-GFP positive areas.
1201 (F) Photosynthetic efficiency (Fv/Fm) in non-infected areas, in thalli from 4 weeks old plants
1202 after 2 weeks of infection, compared to equivalent areas from mock treated plants. 5

1203 biological and 10 technical replicates for each were assayed in both infected and mock
1204 treated plants. Statistical assessment was performed using a two-sided parametric T-
1205 test. Length of the whiskers: 1.5 x IQR. Central line: median. Box width: IQR (i.e. Q3-Q1).
1206 Source data are provided as a Source data File. Marchantia plants and cameras depicting
1207 measured areas come from Biorender. Light green area indicated TMV-GFP positive
1208 areas.

1209 **Figure 4**. Salicylic and jasmonate signalling pathways are activated during Marchantia-TMV
1210 interaction.

1211 (A) Venn diagrams showing the overlap between the transcriptional responses under TMV
1212 infection ad a salicylic treatment time course (2 and 6 hours).
1213 (B) Overlap between the trancriptome responses to TMV and Mpjaz1ko mutants with
1214 constitutively active jasmonate signalling (left), and treatment with the active dn-OPDA
1215 jasmonate (right).
1216 (C) Overlap between the trancriptome responses commonly found in TMV infection and the
1217 different hormone-related transcriptomes.
1218 (D) Biological processes to which genes commonly upregulated in response to TMV
1219 infection, SA treatment (2,6 and 12h) and activation of jasmonate signalling belong
1220 (E) Biological processes to which genes commonly downregulated in response to TMV
1221 infection, SA treatment (12h) and activation of jasmonate signalling belong.
1222 (F) Biological processes to which commonly upregulated in response to TMV infection, SA
1223 treatment (6 h) and activation of jasmonate signalling in Mpjaz1KO plants belong.
1224 (G) Biological processes to which commonly upregulated in response to TMV infection, SA (6
1225 h) and dn-OPDA treatments belong.

1226 Results in panels 4D-G come from a hypergeometric method with BY (BenjaminiYekutieli) p
1227 adjustment with minimal size of genes annotated for testing of 5 and p-value cutoff of 0.05.

1228 **Figure 5.** TMV infection triggers maturation and aging in Marchantia.

1229 (A) Pairwise comparison between transcriptomes from mock and TMV samples along with
1230 those from sliced thallus samples. Slice 1(S1) corresponds to the top of thalli (youngest
1231 part), while slice 6 (S6), corresponds to the base of thalli encompassing the oldest part.
1232 (B) Pairwise comparison between transcriptomes from mock and TMV samples along with
1233 those from Marchantia developmental series Day 1 (D1) samples correspond to 1 day

1234 after germination (youngest), while day 31 (31D) corresponds to fully mature Marchantia
1235 thalli 31 days after germination.

1236 **Figure 6.** Conservation of the interaction between Marchantia and the TMV silencing suppressor
1237 p126.

1238 (A) p126-GFP shows accumulation in the cytoplasm of Marchantia cells in cross-sections of
1239 thalli from 4 weeks old plants (right) compared to thalli from untransformed plants of
1240 the same age plants (left). The pictures show the merge between green (GFP) and red
1241 (autofluorescence) channels. P stands for Photosynthetic region, S for storage region and
1242 E stands for lower epidermis. Merge was performed using Fiji Scale bars are 100 µMs.
1243 (B) Overexpression of p126 inhibits growth (area) when compared to Tak-1 control plants.
1244 Analysis was done in 4 weeks old plants in 3 biological replicates (n=12). Statistical
1245 significance was assessed using a two-sided Wilcoxon-test with Holm p adjustment.
1246 Length of the whiskers: 1.5 x IQR. Central line: median. Box width: IQR (i.e. Q3-Q1).
1247 (C) MpNAC7 interacts with the helicase domain of p126 in yeast.
1248 (D) MpNAC7 and ATAF2 interact both with the helicase and the full length p126 in planta.
1249 (E) Transient expression of MpNAC7 in Nicotiana plants abrogates local and systemic TMV
1250 infection. TMV presence is shown as purple.

1251

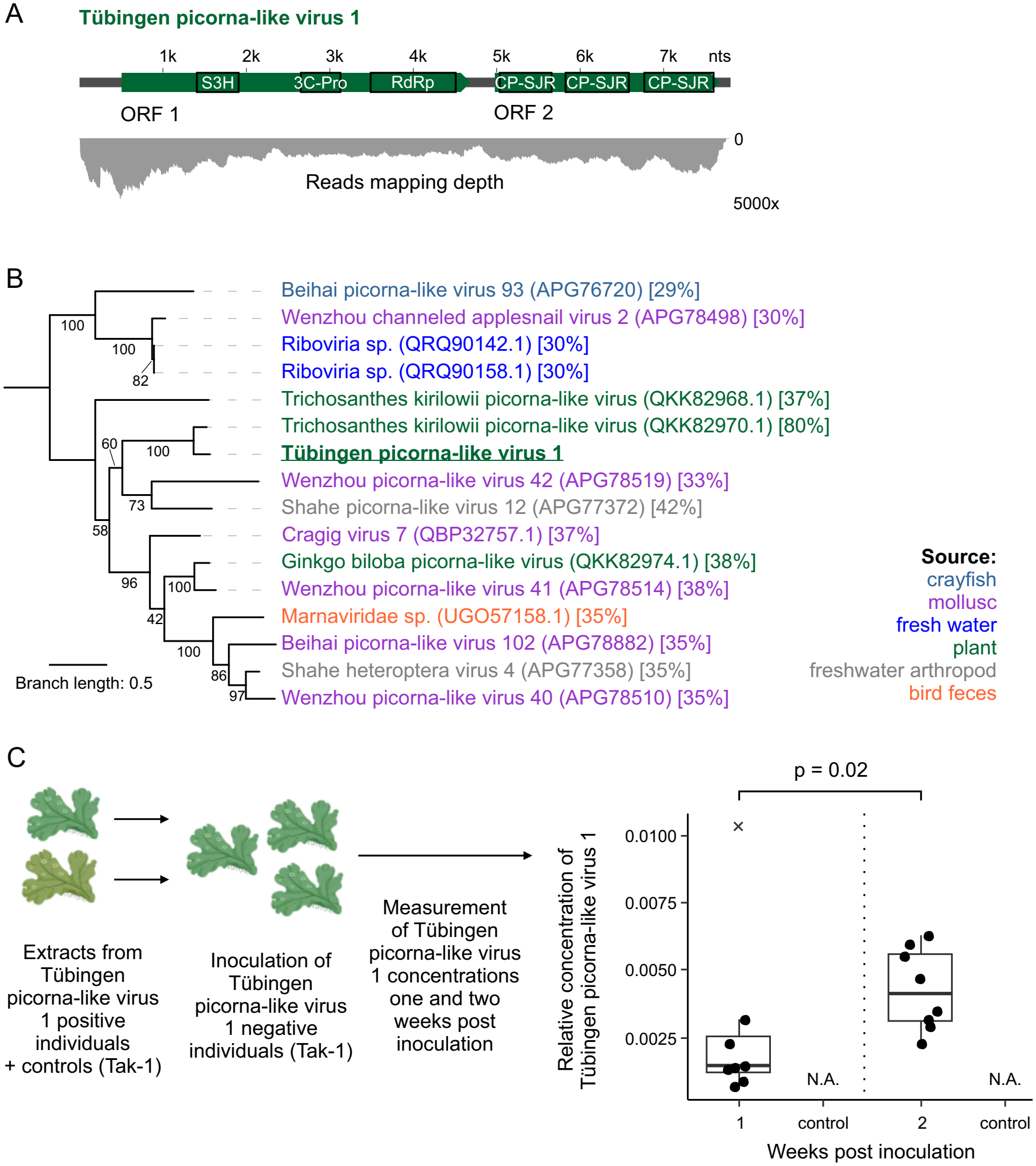
A
Tübingen picorna-like virus 1
1k
2k
3k
4k
5k
6k
7k
nts
S3H
3C-Pro
RdRp
CP-SJR
CP-SJR
CP-SJR
ORF 1
ORF 2
0
Reads mapping depth
5000x
B
Beihai picorna-like virus 93 (APG76720) [29%]
Wenzhou channeled applesnail virus 2 (APG78498) [30%]
Riboviria sp. (QRQ90142.1) [30%]
Riboviria sp. (QRQ90158.1) [30%]
Trichosanthes kirilowii picorna-like virus (QKK82968.1) [37%]
Trichosanthes kirilowii picorna-like virus (QKK82970.1) [80%]
Tübingen picorna-like virus 1
Wenzhou picorna-like virus 42 (APG78519) [33%]
Shahe picorna-like virus 12 (APG77372) [42%]
Cragig virus 7 (QBP32757.1) [37%]
Ginkgo biloba picorna-like virus (QKK82974.1) [38%]
Wenzhou picorna-like virus 41 (APG78514) [38%]
Marnaviridae sp. (UGO57158.1) [35%]
Beihai picorna-like virus 102 (APG78882) [35%]
Shahe heteroptera virus 4 (APG77358) [35%]
Wenzhou picorna-like virus 40 (APG78510) [35%]
100
100
82
60
100
73
58
96
100
42
100
86
97
Branch length: 0.5
Source:
crayfish
mollusc
fresh water
plant
freshwater arthropod
bird feces
C
Extracts from Tübingen picorna-like virus 1 positive individuals + controls (Tak-1)
Inoculation of Tübingen picorna-like virus 1 negative individuals (Tak-1)
Measurement of Tübingen picorna-like virus 1 concentrations one and two weeks post inoculation
p = 0.02
Relative concentration of Tübingen picorna-like virus 1
0.0100
0.0075
0.0050
0.0025
N.A.
N.A.
1
control
2
control
Weeks post inoculation

A

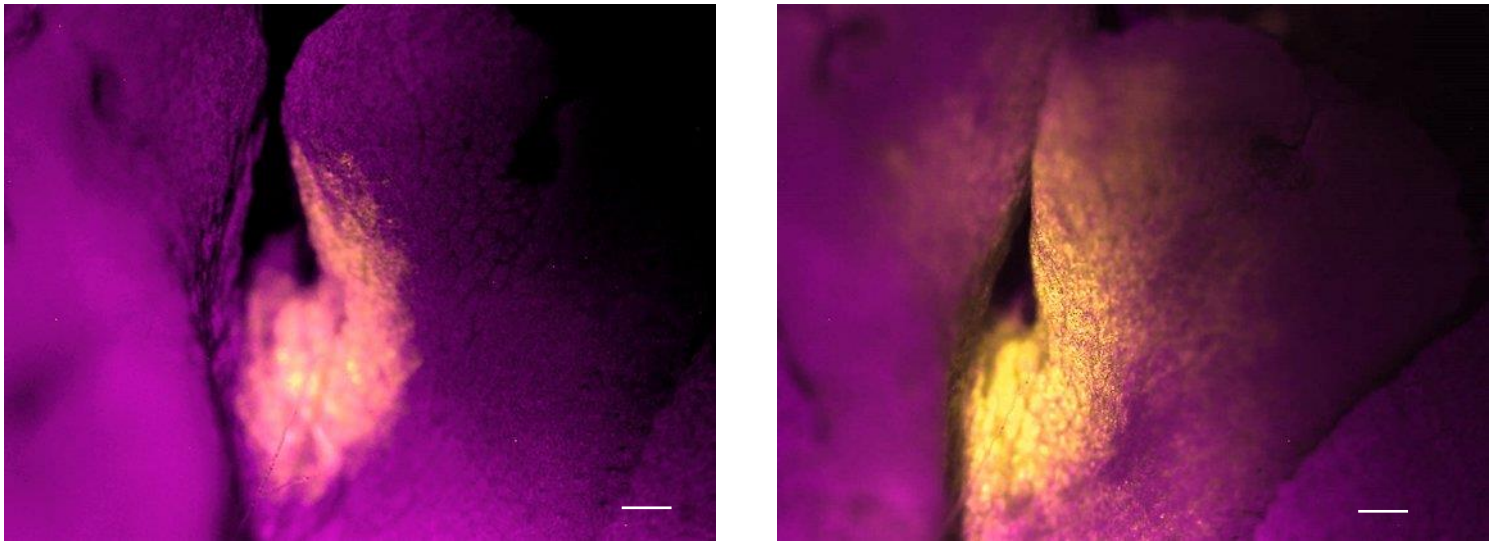

B

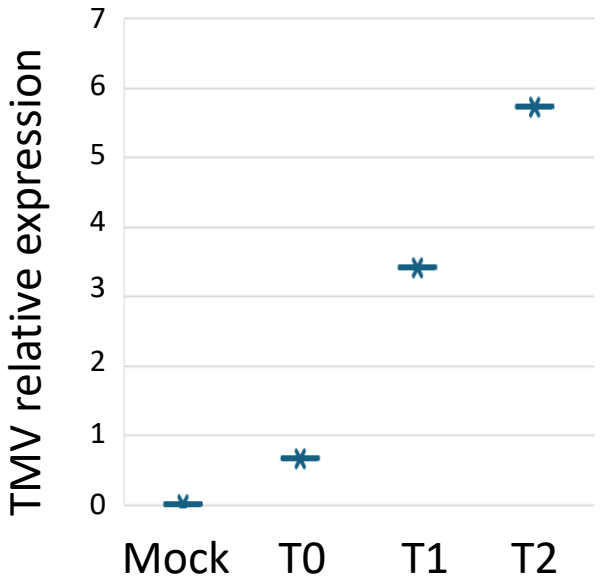

C

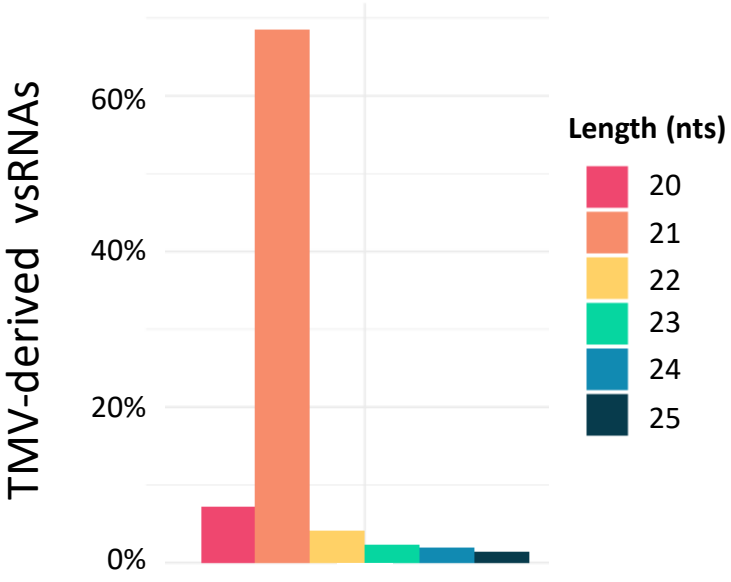

D

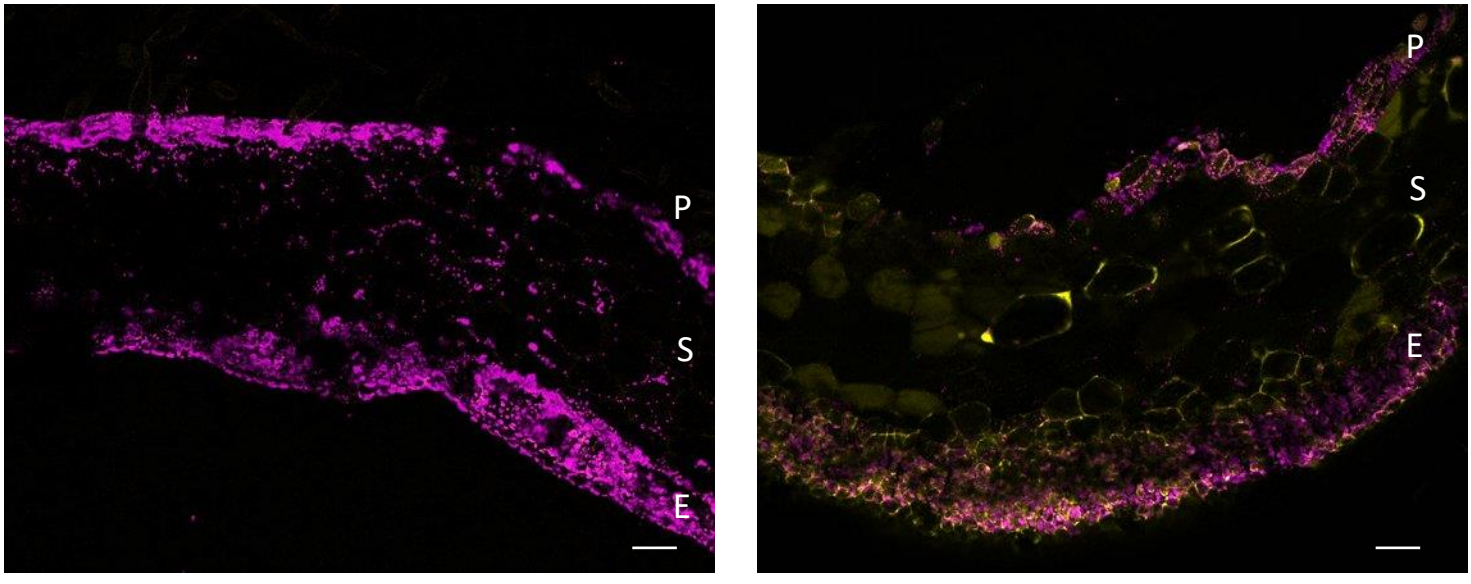

Mock TMV-GFP

A ***PTI Marker genes***

Name	ID	Relative expression level	padj
MpPR9	Mp5g21510	4.04	1.18E-21
MpSYP13B	Mp2g21910	2.34	0.00089
MpCML42	Mp6g18000	1.79	3.01E-17
MpWRKY22	Mp7g17200	1.74	1.82E-32
MpACRE132	Mp1g27170	1.22	1.30E-10

B ***Wound and TMV responsive ERFs***

Name	ID	Relative expression level	padj
MpERF1	Mp7g09350	4.24	0.28
MpERF21	Mp5g22160	1.68	5.91E-05
MpERF8	Mp6g18650	1.48	1.33E-41
MpERF18	Mp5g12480	1.14	0.0015
MpERF15	Mp7g09350	1.06	0.028
MpAP2L1	Mp8g11450	-1.62	4.18E-13
MpERF10	Mp7g00860	-2.83	9.05E-11
MpERF17	Mp4g22280	-2.38	0.00058
MpERF12	Mp6g06870	-2.95	0.014
MpERF16	Mp4g22290	-3.11	0.0004
MpERF13	Mp6g08690	-3.25	4.72E-05

C

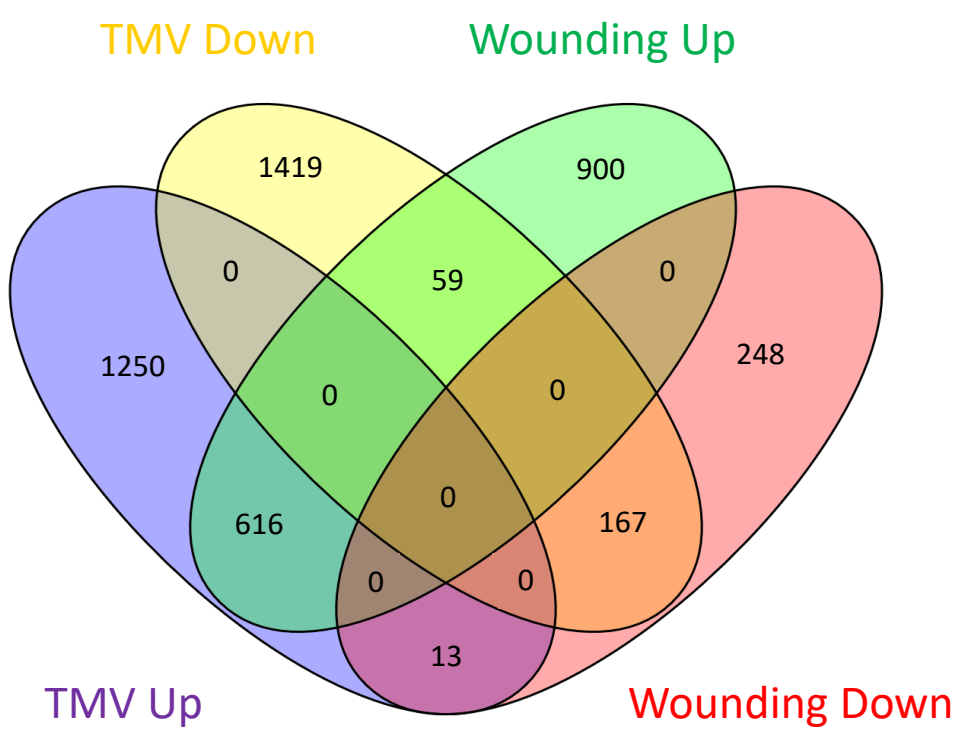

D ***Chitin and TMV responsive WRKYs***

Name	ID	Relative expression level	padj
MpWRKY7	Mp3g17660	3.56	1.68E-34
MpWRKY6	Mp1g08960	2.52	3.71E-17
MpWRKY12	Mp4g00200	1.89	1.90E-11
MpWRKY10	Mp7g06550	1.79	7.31E-06
MpWRKY9	Mp7g17200	1.74	1.82E-32
MpWRKY13	Mp4g00180	1.64	7.72E-11
MpWRKY1	Mp3g00010	1.28	3.79E-25
MpWRKY14	Mp6g16800	1.16	0.013

E ***Infected area***

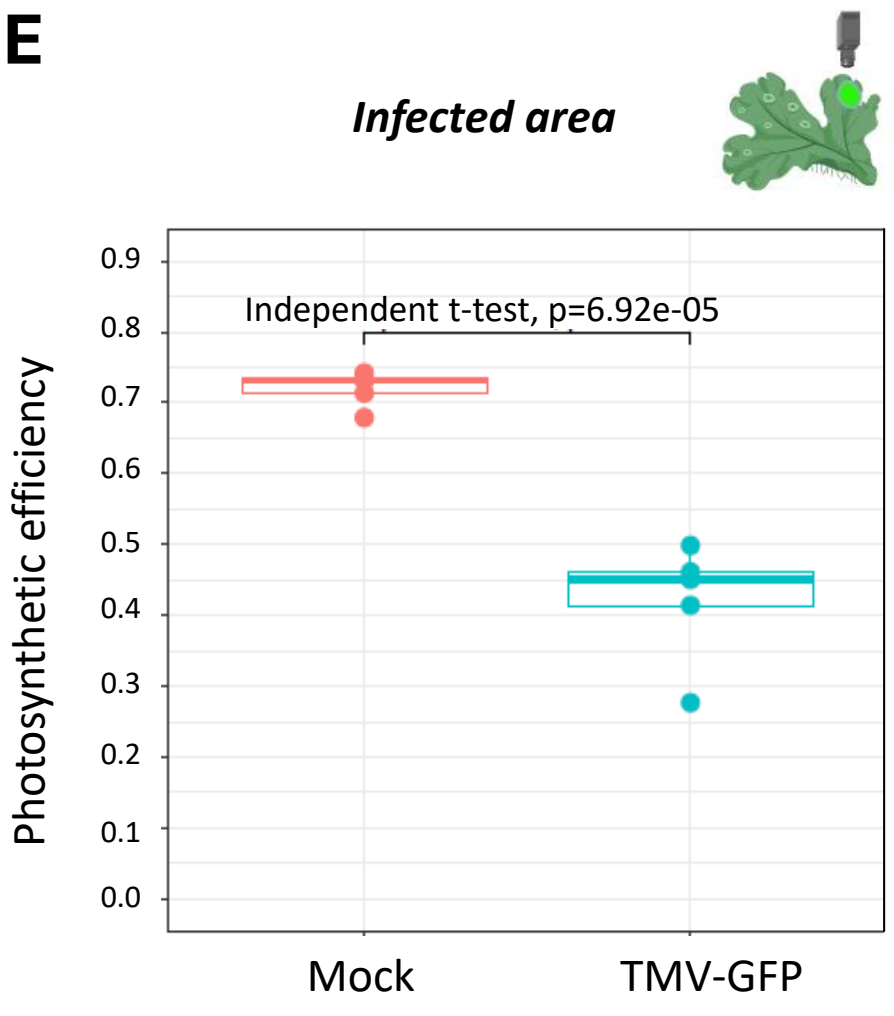

F ***Non-infected area***

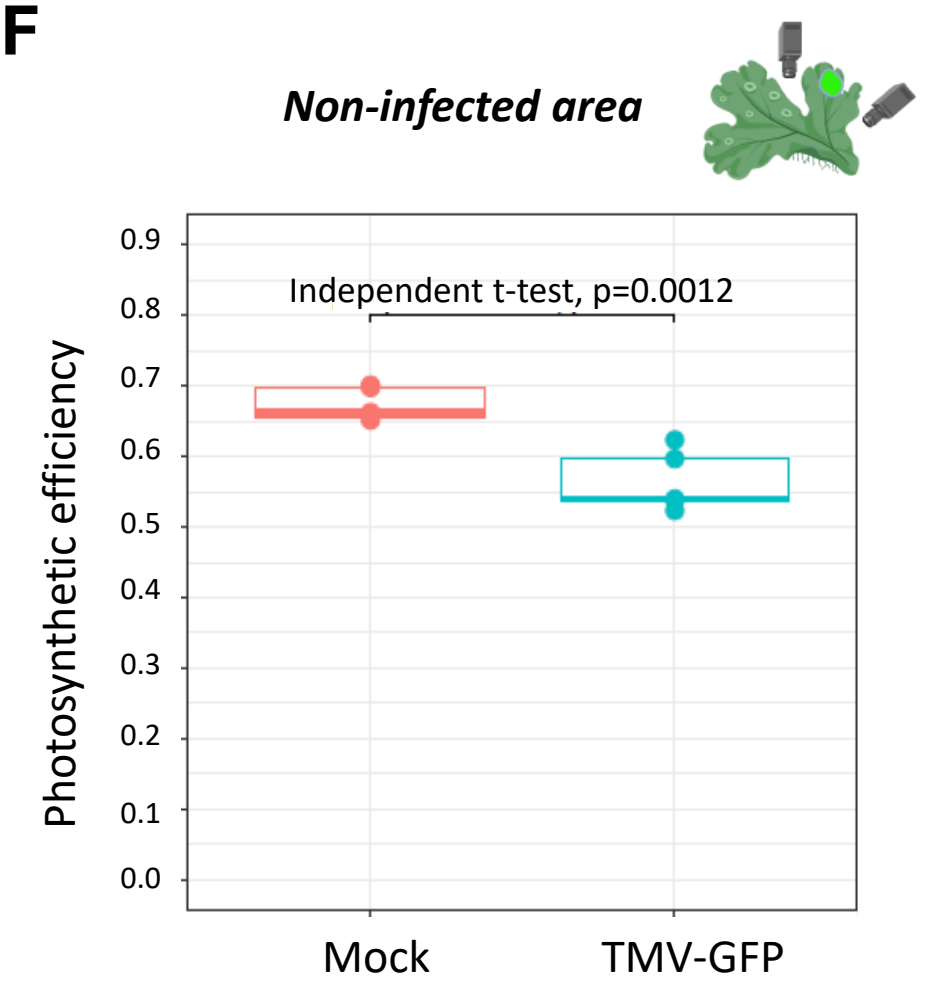

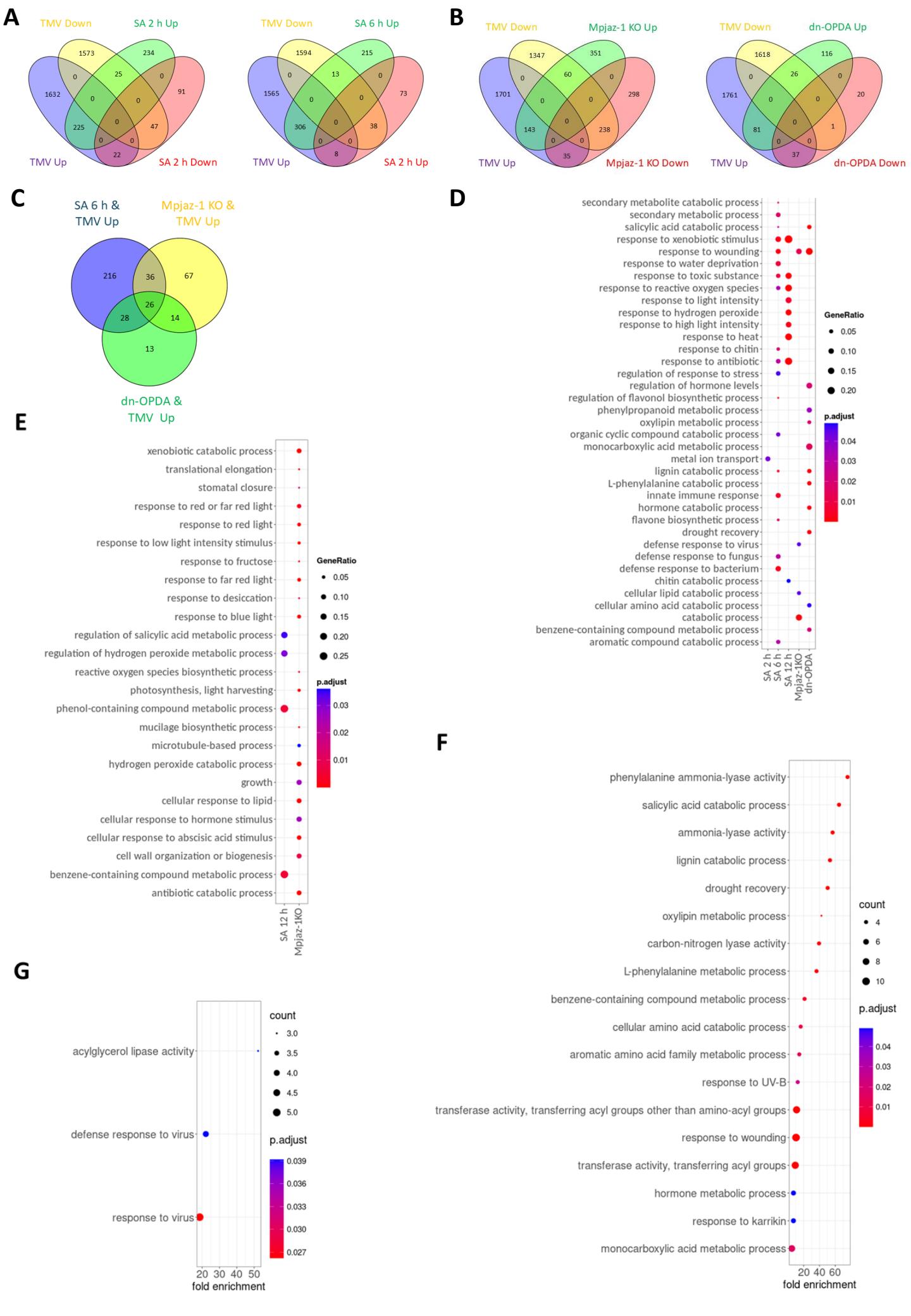
A
TMV Down
SA 2 h Up
TMV Up
SA 2 h Down
1573
234
1632
25
91
225
47
22
TMV Down
SA 6 h Up
TMV Up
SA 2 h Up
1594
215
1565
13
73
306
38
8
B
TMV Down
Mpjaz-1 KO Up
TMV Up
Mpjaz-1 KO Down
1347
351
1701
60
298
143
238
35
TMV Down
dn-OPDA Up
TMV Up
dn-OPDA Down
1618
116
1761
26
20
81
1
37
C
SA 6 h & TMV Up
Mpjaz-1 KO & TMV Up
dn-OPDA & TMV Up
216
36
67
26
28
14
13
D
secondary metabolite catabolic process
secondary metabolic process
salicylic acid catabolic process
response to xenobiotic stimulus
response to wounding
response to water deprivation
response to toxic substance
response to reactive oxygen species
response to light intensity
response to hydrogen peroxide
response to high light intensity
response to heat
response to chitin
response to antibiotic
regulation of response to stress
regulation of hormone levels
regulation of flavonol biosynthetic process
phenylpropanoid metabolic process
oxylipin metabolic process
organic cyclic compound catabolic process
monocarboxylic acid metabolic process
metal ion transport
lignin catabolic process
L-phenylalanine catabolic process
innate immune response
hormone catabolic process
flavone biosynthetic process
drought recovery
defense response to virus
defense response to fungus
defense response to bacterium
chitin catabolic process
cellular lipid catabolic process
cellular amino acid catabolic process
catabolic process
benzene-containing compound metabolic process
aromatic compound catabolic process
SA 2 h
SA 6 h
SA 12 h
Mpjaz-1KO
dn-OPDA
GeneRatio
0.05
0.10
0.15
0.20
p.adjust
0.04
0.03
0.02
0.01
E
xenobiotic catabolic process
translational elongation
stomatal closure
response to red or far red light
response to red light
response to low light intensity stimulus
response to fructose
response to far red light
response to desiccation
response to blue light
regulation of salicylic acid metabolic process
regulation of hydrogen peroxide metabolic process
reactive oxygen species biosynthetic process
photosynthesis, light harvesting
phenol-containing compound metabolic process
mucilage biosynthetic process
microtubule-based process
hydrogen peroxide catabolic process
growth
cellular response to lipid
cellular response to hormone stimulus
cellular response to abscisic acid stimulus
cell wall organization or biogenesis
benzene-containing compound metabolic process
antibiotic catabolic process
SA 12 h
Mpjaz-1KO
GeneRatio
0.05
0.10
0.15
0.20
0.25
p.adjust
0.03
0.02
0.01
F
phenylalanine ammonia-lyase activity
salicylic acid catabolic process
ammonia-lyase activity
lignin catabolic process
drought recovery
oxylipin metabolic process
carbon-nitrogen lyase activity
L-phenylalanine metabolic process
benzene-containing compound metabolic process
cellular amino acid catabolic process
aromatic amino acid family metabolic process
response to UV-B
transferase activity, transferring acyl groups other than amino-acyl groups
response to wounding
transferase activity, transferring acyl groups
hormone metabolic process
response to karrikin
monocarboxylic acid metabolic process
20 40 60
fold enrichment
count
4
6
8
10
p.adjust
0.04
0.03
0.02
0.01
G
acylglycerol lipase activity
defense response to virus
response to virus
20 30 40 50
fold enrichment
count
3.0
3.5
4.0
4.5
5.0
p.adjust
0.039
0.036
0.033
0.030
0.027

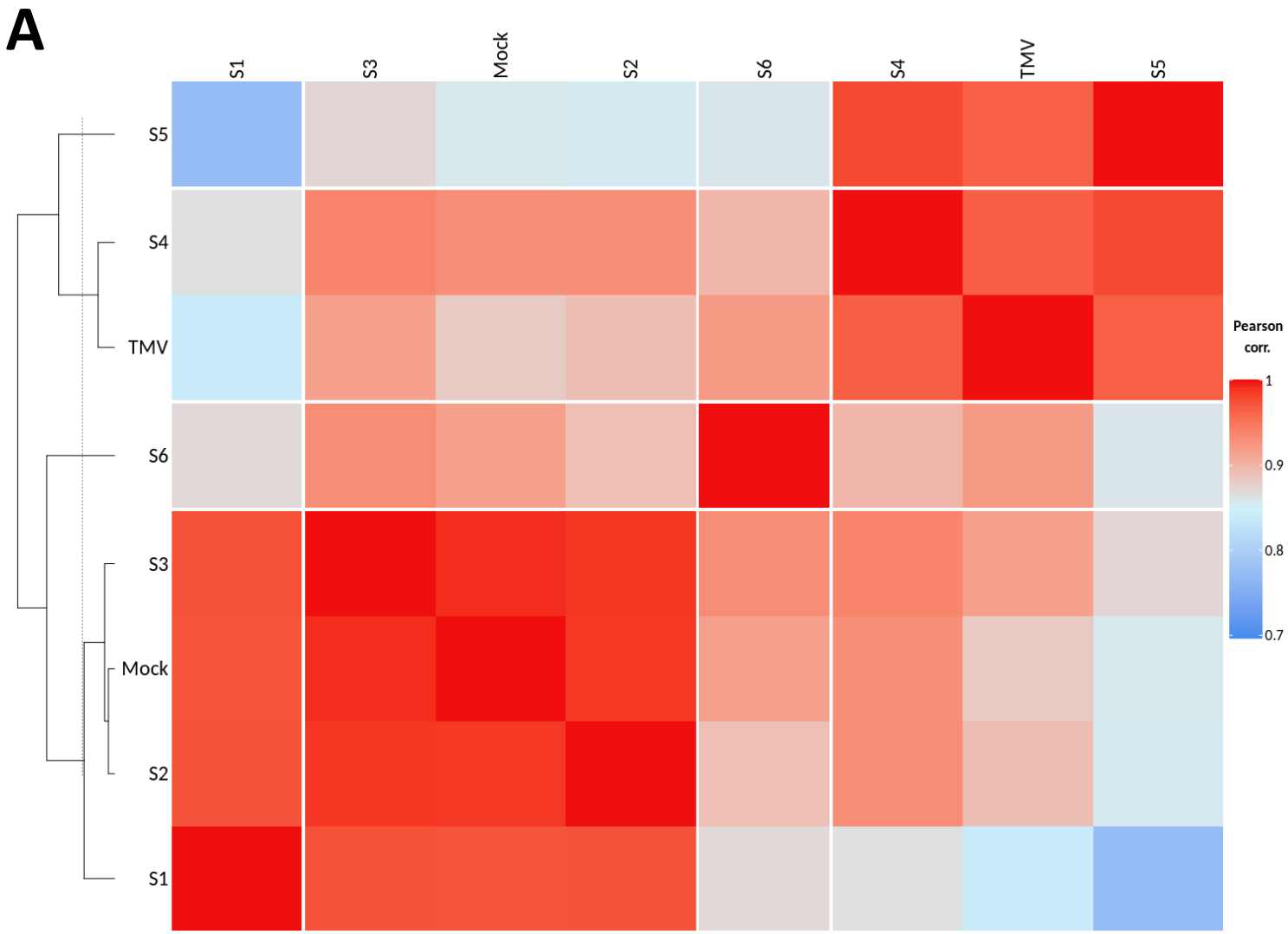
A
S1
S3
Mock
S2
S6
S4
TMV
S5
S5
S4
TMV
S6
S3
Mock
S2
S1
Pearson corr.
1
0.9
0.8
0.7

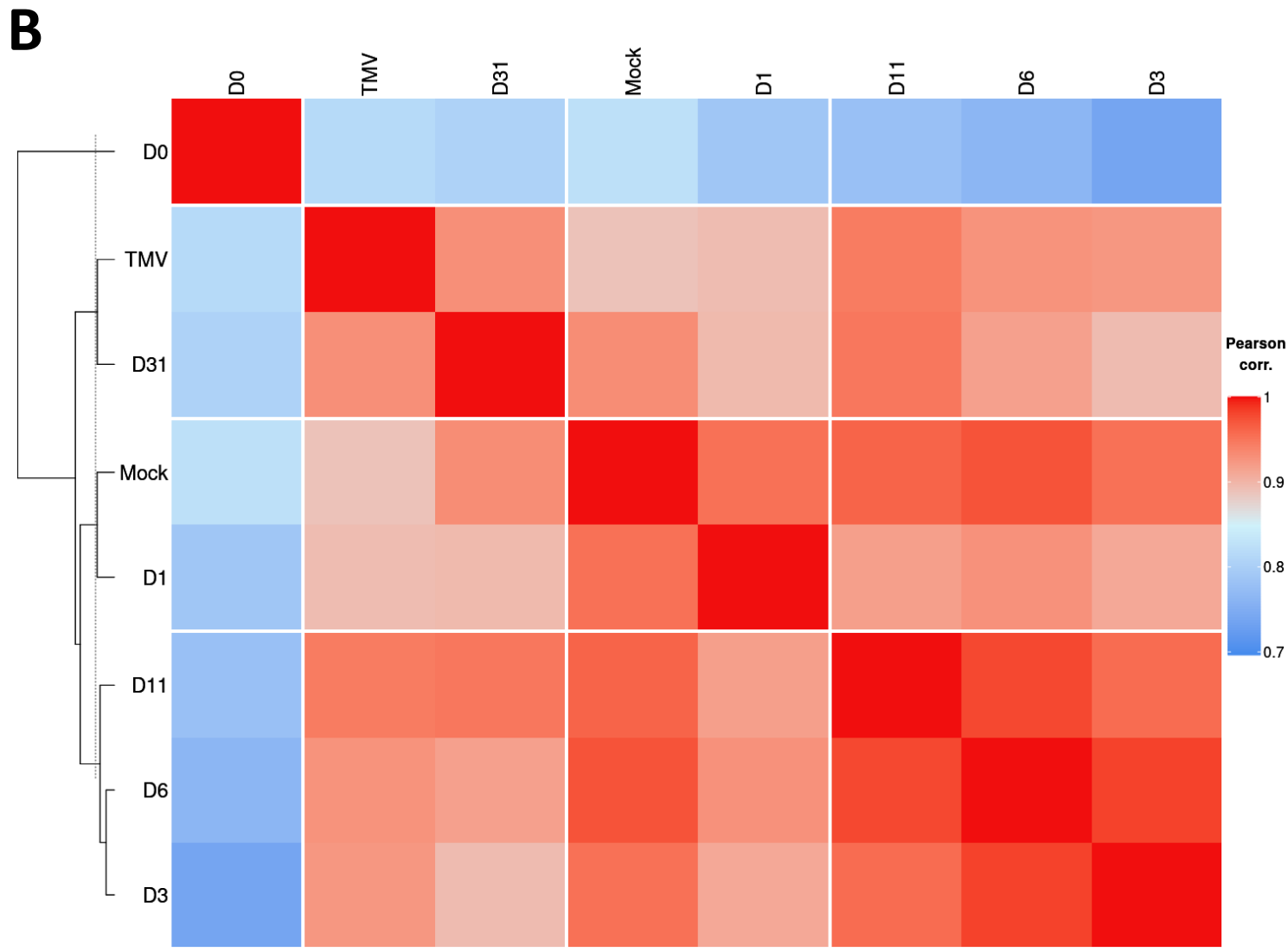
B
D0
TMV
D31
Mock
D1
D11
D6
D3
D0
TMV
D31
Mock
D1
D11
D6
D3
Pearson corr.
1
0.9
0.8
0.7

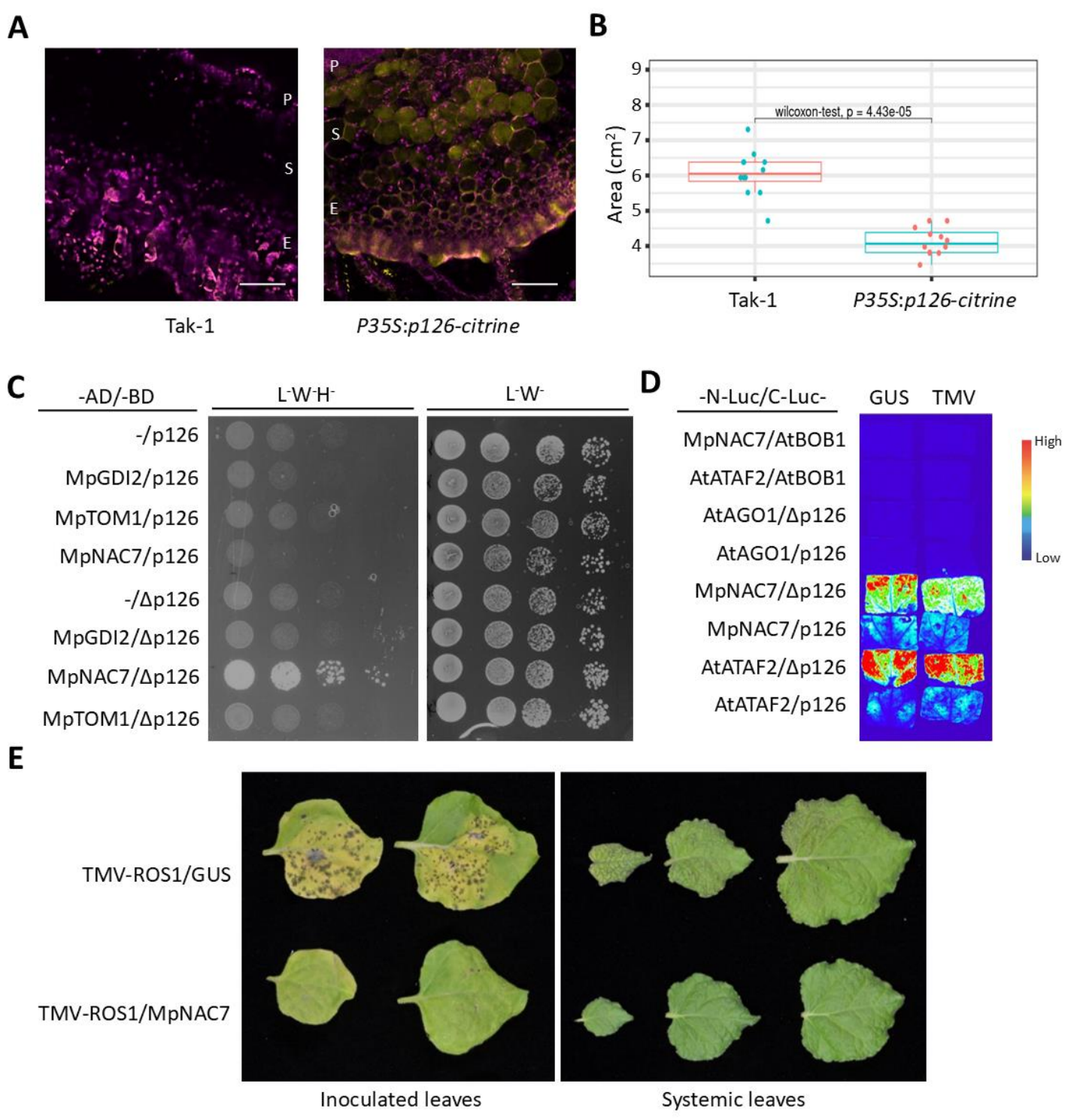
A
P
S
E
Tak-1
P35S:p126-citrine
B
wilcoxon-test, p = 4.43e-05
Area (cm²)
9
8
7
6
5
4
Tak-1
P35S:p126-citrine
C
-AD/-BD
L-W-H-
L-W-
-/p126
MpGDI2/p126
MpTOM1/p126
MpNAC7/p126
-/Δp126
MpGDI2/Δp126
MpNAC7/Δp126
MpTOM1/Δp126
D
-N-Luc/C-Luc-
GUS
TMV
MpNAC7/AtBOB1
AtATAF2/AtBOB1
AtAGO1/Δp126
AtAGO1/p126
MpNAC7/Δp126
MpNAC7/p126
AtATAF2/Δp126
AtATAF2/p126
High
Low
E
TMV-ROS1/GUS
TMV-ROS1/MpNAC7
Inoculated leaves
Systemic leaves